REVIEW

National Science Review
4: 453–489, 2017
doi: 10.1093/nsr/nwx009
Advance access publication 2 March 2017

MATERIALS SCIENCE

Carbon-based supercapacitors for efficient energy storage

Xuli Chen, Rajib Paul and Liming Dai*

ABSTRACT

The advancement of modern electronic devices depends strongly on the highly efficient energy sources possessing high energy density and power density. In this regard, supercapacitors show great promise. Due to the unique hierarchical structure, excellent electrical and mechanical properties, and high specific surface area, carbon nanomaterials (particularly, carbon nanotubes, graphene, mesoporous carbon and their hybrids) have been widely investigated as efficient electrode materials in supercapacitors. This review article summarizes progress in high-performance supercapacitors based on carbon nanomaterials with an emphasis on the design and fabrication of electrode structures and elucidation of charge-storage mechanisms. Recent developments on carbon-based flexible and stretchable supercapacitors for various potential applications, including integrated energy sources, self-powered sensors and wearable electronics, are also discussed.

Keywords: electric double-layer supercapacitors, pseudocapacitors, hybrid supercapacitors, carbon nanotube (CNT), graphene, flexible and wearable electronics

INTRODUCTION

The ever increasing consumption of fossil fuels and their soaring price have caused serious concerns about the fast depletion of existing fossil-fuel reserves and the associated alarming greenhouse-gas emissions and pollutions in air and on soil. Therefore, it is important to develop environment friendly energy-generation and storage technologies. In particular, there has recently been intensive attention on the advancement of energy-storage devices, including electrochemical supercapacitors and batteries [1–7]. Compared to batteries, electrochemical supercapacitors (ESCs) are capable of providing 100–1000 times higher power density, but with 3–30 times lower energy density [8]. As a consequence, ESCs are particularly useful for high power bursts, for example for accelerating/breaking high-speed transportation systems. Moreover, ESCs can sustain up to millions of charge/discharge cycles via the electric double-layer charge storage free from chemical reactions. In contrast, batteries suffer from volumetric modulation and swelling of active materials in the electrodes due to the excessive redox reactions during charge/discharge cycles [8]. As far as the safety issues are concerned, therefore, supercapacitors are much more reliable than batteries. In order to minimize/avoid possible decomposition of the electrolyte, however, the operating voltage for ESCs must be low as compared to batteries. Nevertheless, a high operating voltage is desirable for ESCs with a high energy density, and hence an optimized operating voltage is essential for high-performance ESCs.

In an electrochemical supercapacitor, two electrodes are kept apart by a separator between them (Fig. 1). These two electrodes are identical for a symmetric supercapacitor (Fig. 1a), but different for an asymmetric supercapacitor (Fig. 1b and c). The separator is generally ion-permeable, but also electrically insulating, soaked with electrolytes to allow ionic charge transfer between the electrodes. Polymer or paper separators are often used with organic electrolytes while ceramic or glass-fiber separators are preferred for aqueous electrolytes [8,9]. Depending on the ways in which energy is stored, ESCs can be divided into electric double-layer capacitors (EDLCs), in which charge storage occurs at the interfaces between the electrolyte and electrodes (Fig. 1a), and pseudocapacitors (PCs), involving reversible and fast Faradaic redox reactions for charge

Center of Advanced Science and Engineering for Carbon (Case 4Carbon), Department of Macromolecular Science and Engineering, Case School of Engineering, Case Western Reserve University, Cleveland, Ohio 44106, USA

*Corresponding author. E-mail: liming.dai@case.edu

Received 24 July 2016; **Revised** 6 September 2016; **Accepted** 13 September 2016

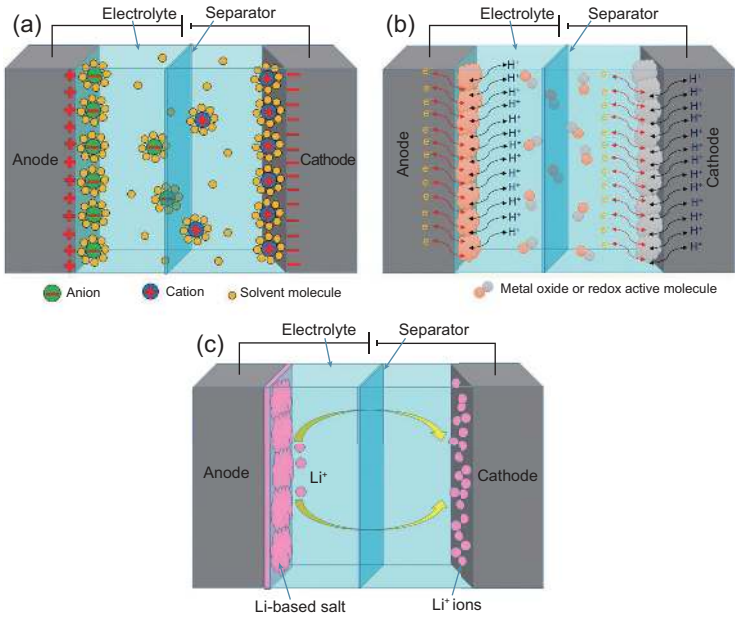

Figure 1. Schematic representation of (a) electrical double-layer capacitor (EDLC), (b) pseudocapacitor (PC) and (c) hybrid supercapacitor (HSC).

storage (Fig. 1b). When a supercapacitor stores charges by matching the capacitive carbon electrode with either a peseudocapacitive or lithium-insertion electrode (Fig. 1c), it is then called a hybrid supercapacitor (HSC). Owing to their availability in large quantities at a relatively low cost, unique hierarchal structures with a large surface/interface area and excellent electrical/electrochemical/mechanical properties, nanoporous and/or mesoporous carbon materials are useful as the electrode materials in all types of ESCs.

Along with the recent rapid development of flexible/wearable electronics, there is an urgent need for integrated power sources based on flexible and even stretchable electrodes. Consequently, flexible and stretchable fiber-shaped or very thin supercapacitors (SCs) have recently attracted a great deal of interest [10]. In this context, carbon nanotubes (CNTs) and graphene with a high mechanical stability and excellent bending strength have been reported to be ideal electrode materials for flexible and stretchable ESCs. Thus, carbon nanomaterials have been widely investigated for developing new electrode materials in various ESCs for efficient energy storage. A huge amount of literature on carbon-based ESCs has been produced, with the number of publications still rapidly increasing every year. A timely review on such a rapidly growing field of such significance is highly desirable. The aim of this article is to provide a timely, concise and critical review by summarizing recent important progress on the topic and presenting critical issues related to the material/electrode design and the elucidation of energy-storage mechanisms. Through such a critical review, our understanding of carbon-based electrode materials for energy storage will significantly increase, as will insights for the future development.

CARBON NANOMATERIALS

Conventional carbon materials are divided into three forms: diamond, graphite and amorphous carbon [1]. Their properties vary depending on the arrangement of carbon atoms. For example, diamond is hard and rigid due to its special diamond cubic crystal structure with sigma bonding between sp^3 hybridized carbon molecules. Having a layered structure with strong covalent bonding between sp^2 hybridized carbon atoms in the plane of individual layers and weak van der Waals interactions between adjacent layers, graphite is soft. The recent development of nanoscience and nanotechnology has opened up a new frontier in carbon materials research by creating new graphitic carbon nanomaterials with multi-dimensions, including dimension-less (0D) fullerene, one-dimensional (1D) carbon nanotubes (CNTs) [11–19] and two-dimensional (2D) graphene [20–31]. Fullerene C_{60} has a soccer-ball-like structure containing 20 carbon hexagons with 12 carbon pentagons formed into a cage of truncated icosahedrons. Fullerene C_{60} is a perfect electron acceptor, which has been widely used in solar cells for charge separation. Due to its intractability, low electrical conductivity and small surface area, fullerene has been rarely used for energy storage with respect to other carbon nanomaterials. So far, CNTs [2,32–42], graphene [29,43–73], mesoporous carbon [74–80] and their hybrids [81–94] have been widely studied as supercapacitor electrodes because of their excellent electrical conductivity, high specific surface area, outstanding electrochemical activity and the ease with which they can be functionalized into multidimensional and multifunctional structures with excellent electrical and mechanical properties.

APPLICATION OF CARBON NANOMATERIALS IN SUPERCAPACITORS

Current research and development on energy-storage devices have been mainly focused on supercapacitors, lithium-ion batteries and other related batteries. Compared with batteries, supercapacitors possess higher power density, longer cyclic stability, higher Coulombic efficiency and shorter period for

full charge–discharge cycles. Thus, supercapacitors, particularly those based on carbon CNTs, graphene and mesoporous carbon electrodes, have gained increasing popularity as one of the most important energy-storage devices.

EDLCs

Similarly to traditional capacitors, EDLCs also store energy through charge separation, which leads to double-layer capacitance. Unlike a traditional capacitor, however, an EDLC contains two separated charge layers at the interfaces of electrolyte with positive electrode and negative electrode, respectively. The separation between electrical double layers in an EDLC is much smaller than that in a conventional capacitor, leading to a several orders of magnitude higher specific capacitance for the EDLC. Since there is no chemical reaction involved and the transport of ions in the electrolyte solution or electrons through the electrodes is responsible for charge storage, EDLCs can be fully charged or discharged within a short time with a high power density. Ideally, EDLCs require electrode materials with a high specific surface area and excellent electrical conductivity, which can be fulfilled especially by CNTs and graphene.

CNTs in EDLCs

CNTs, with and without compositing with other electrode materials, are highly suitable for supercapacitor electrodes. The reported specific surface area of pure CNTs is in between 120 and 500 m^2/g with the specific capacitance ranging from 2 F/g to 200 F/g [2,32–34]. Using single-walled carbon nanotubes (SWNTs) as the electrode materials, a specific capacitance, power density and energy density up to 180 F/g, 20 kW/kg and 7 Wh/kg, respectively, have been reported [35,36]. The specific surface area can be enhanced by activating the CNT walls and/or tips. For example, Pan *et al.* have improved the specific surface area of SWNTs from 46.8 m^2/g to 109.4 m^2/g through electrochemical activation, leading to a three-times increase in the specific capacitance [37]. Hata and coworkers have reported a specific surface area of 1300 m^2/g for highly pure SWNTs [38]. Using organic electrolyte (1 M Et_4NBF_4/propylene carbonate) to ensure a high voltage of 4 V, these authors have reported an energy density as high as 94 Wh/kg (or 47 Wh/L) and a power density up to 210 kW/kg (or 105 kW/L).

CNT diameters play a key role in controlling the intrinsic surface area. It was reported that the specific surface area of multiwall carbon nanotubes (MWNTs) with outer diameter of 10∼20 nm and inner diameter of 2∼5 nm varied from 128 to 411 m^2/g with increasing diameters, and the MWNTs exhibited the highest specific capacitance of 80 F/g in 6 M KOH electrolyte [39]. So far, many of the reported EDLCs based on pure CNTs showed high-rate capabilities and cyclic stabilities, together with rectangular cyclic voltammograms and symmetric triangular galvanostatic charge–discharge profiles, indicating high performance for charge storage.

Apart from improving the specific surface area, much effort has been made to improve the electrical conductivity and increase the active sites on CNTs. Heteroatom doping has been demonstrated to be an important and efficient technique for these purposes. For instance, nitrogen-doped (N-doped) CNTs were synthesized by in-situ polymerization of aniline monomers on CNTs, followed by carbonization of polyaniline (PANI)-coated CNTs [40]. In this study, the N-doping level was controlled by adjusting the amount of aniline used, leading to a highest specific capacitance of 205 F/g in 6 M KOH electrolyte—a much higher value than 10 F/g for the pristine CNTs, at 8.64% (by mass) nitrogen doping. Moreover, 97.1% of the initial capacitance was maintained after 1000 cycles. Recently, Gueon and Moon prepared N-doped CNT-based spherical particles by emulsion-assisted evaporation of hexadecane, followed by N-doping using melamine [41]. A specific capacitance of 215 F/g was achieved at a current density of 0.2 A/g—3.1 times the enhancement as compared to that of the pristine CNTs. The observed performance improvement was attributed to the combination of more active sites with a higher electrical conductivity induced by N-doping. Interestingly, N-doped aligned CNT arrays have also been synthesized and systematically characterized for their application in supercapacitors [42]. It was found that the supercapacitor performance at a low scan rate was highly dependent on the pyridinic nitrogen content in N-doped CNTs due to the net charges induced onto the neighboring carbon atoms through protonation of the pyridinic nitrogen.

Graphene in EDLCs

Having the basic carbon lattice structure similar to CNTs with all carbon atoms exposed at the surface, the single-atom-thick 2D graphene sheets show similar electrical and other properties to CNTs, but with an even larger specific surface area [1,2]. Like CNTs, therefore, graphene sheets have also been extensively studied as electrode materials in ESCs. The availability of graphene oxide (GO) by acid

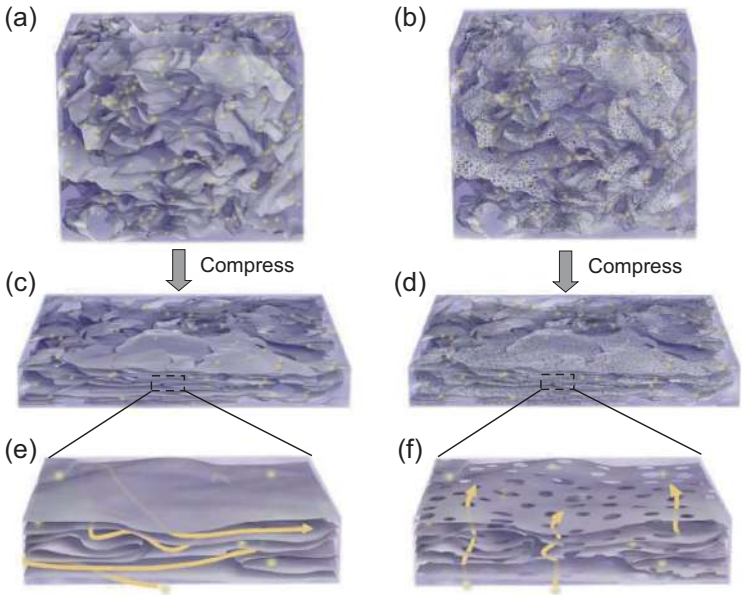

Figure 2. Schematic illustration of the graphene and holey graphene foams. (a, b) Initial 3D macroporous (a) graphene foam and (b) holey graphene foam. (c, d) Compressed films of the (c) graphene foam and (d) holey graphene foam. (e, f) A closed-up view of (e) graphene and (f) holey graphene films. The arrows highlighted the ion transport pathway. Reproduced with permission from ref. [49]. Copyright of Macmillan Publishers Ltd (2014).

oxidation of graphite [43–45], followed by chemical reduction [29,43–45], provides an effective approach for low-cost mass production of reduced graphene oxide (RGO), which can directly be used as EDLC electrode materials. In this regard, Stoller *et al.* used hydrazine hydrate as the reducing reagent to produce RGO from GO [29]. The resultant RGO exhibited a specific capacitance of 135 F/g and specific surface area of 705 m^2/g [29], which is much lower than the theoretic value of 2630 m^2/g, presumably due to RGO aggregation. To minimize the RGO aggregation, Chen and coworkers synthesized graphene with mesoporous structure through thermal exfoliation of RGO at 1050°C to produce a specific capacitance up to 150 F/g in 30% KOH aqueous solution [46]. Microwave irradiation in vacuum can reduce the reduction temperature required for thermal exfoliation, as demonstrated by Lv *et al.* [47]. These authors decreased the exfoliation temperature down to 200°C with a concomitant increase in the specific capacitance up to 264 F/g [47]. By using microwave radiation to assist the exfoliation process, Zhu *et al.* also effectively deducted the exfoliation time to as short as 1 min and the produced graphene could still exhibit specific capacitance of 191 F/gin 5 M KOH [48].

For conventional graphene and RGO electrodes, electrolyte ions can only transfer charges between graphene sheets, which inevitably leads to a much longer ion-transport path with respect to ions transferring through the graphene sheets (Fig. 2). To address this issue, Xu *et al.* synthesized holy graphene sheets, which allow ions to pass through the holes with a minimized transport path while still maintaining the electron-transport efficiency [49]. As a result, their hierarchically structured three-dimensional (3D) holy graphene electrode exhibited both high gravimetric and volumetric specific capacitances of 298 F/g and 212 F/cm^3, respectively. Moreover, the energy density for a corresponding fully packaged supercapacitor is as high as 35 Wh/kg (49 Wh/L), which is sufficient to bridge the gap between supercapacitors and batteries.

Similarly to CNTs, surface activation can also be used to improve the specific capacitance of graphene electrodes without a detrimental effect on the electrical conductivity. Of particular interest, Ruoff and coworkers obtained a dramatically improved specific surface area up to 3100 m^2/g by activating exfoliated GO with KOH [50], which is even higher than the theoretically predicted specific surface area of monolayer graphene (2630 m^2/g) and attributable to the presence of a 3D network containing pores with sizes of 1∼10 nm. In another study, the same group activated RGO films to produce graphene films of a specific capacitance of 120 F/g at high current density of 10 A/g with corresponding energy density and power density of 26 Wh/kg and 500 kW/kg, respectively [51]. Later, they further improved the specific surface area up to 3290 m^2/g by designing a mesoporous structure integrated with macroporous scaffolds [52]. As a result, specific capacitance of 174 F/g (100 F/cm^3) was achieved with energy density and power density of 74 Wh/kg and 338 kW/kg, respectively.

Doping graphene with hetero atoms can also improve its electrical/electrochemical properties for energy storage and many other applications [53]. Indeed, Jeong *et al.* synthesized N-doped graphene through a simple plasma process [54], and the N-doped graphene thus produced was found to exhibit a specific capacitance of 280 F/g, which is four times higher than that of the corresponding undoped pristine graphene. This is because N-doping can introduce charge-transferring sites through doping-induced charge modulation and improve electrical conductivity of graphene, and hence the improved specific capacitance, along with an enhanced power density of 8×10^5 W/kg and energy density of 48 Wh/kg. N-doped graphene can also be synthesized through hydrothermal reduction of GO with nitrogen containing chemicals [55]. The resultant 3D N-doped graphene framework has a very low density of 2.1 mg/cm^3 with a high specific capacitance of 484 F/g in 1 M $LiClO_4$ electrolyte and maintains 415 F/g capacitance after 1000 cycles at a high

current density of 100 A/g [55]. Similarly, doping graphene with other elements, such as boron, phosphorous and/or co-doping with N and P or B and N, has also been demonstrated to significantly improve their energy-storage performance [56,57].

Graphene-based self-assembled 3D structures (such as hydrogels and aerogels) have recently emerged as electrode materials for supercapacitors due to their high porosity, low density and excellent adsorption capacity [58–60]. The detailed synthetic processes and properties of graphene hydrogels and aerogels have been reviewed in references [58–60]. Briefly, in an aqueous solution of GO, the van der Waals attractions from the basal planes of GO sheets and the electrostatic repulsions from the functional groups of GO sheets are balanced each other to maintain the well-dispersed state of GO sheets. While this balance is lost, gelation of the GO dispersion takes place, leading to the formation of 3D GO hydrogels that can be further reduced or functionalized to produce 3D graphene-based architectures [61–63]. Different techniques have been used to produce graphene hydrogels, such as hydrothermal reduction [61], chemical reduction [63], cross-linking agent (including metal ions [64], biomolecules [65], polymers [66] etc.), sol-gel reaction [67], freeze-drying [68] and so on. Similarly to hydrogels, graphene aerogels are made through replacing the solution part with a gas [69–70]. There have been numerous studies on graphene aerogels for supercapacitor applications. Such successful efforts have been summarized in Table 1. For assemblies of graphene hydrogels, aerogels or organogels [71], their overall conductivities are generally poor.

As the graphene-based nanostructured carbon materials often offer low density, in most cases, the volumetric energy densities of carbon-based supercapacitors are low, which hinders their practical application. Yang *et al.* and Yoon *et al.* have demonstrated graphene-based highly packed supercapacitors with volumetric energy density of 59.9 Wh/L and specific capacitance of 171 F/cm^3, respectively [72,73]. However, much more effort must be made in improving the volumetric energy density.

Mesoporous carbon in EDLCs

Activated carbon has been widely used as electrodes in energy-storage devices because of their easy synthesis, low cost and acceptable electrical conductivity. However, these advantages are hindered by its low effective specific surface area due to the presence of randomly connected micropores with size less than 2 nm that are hardly accessible by electrolyte ions [2]. To address this issue, mesoporous carbon of a larger pore diameter (2–50 nm) was explored as a supercapacitor electrode with a high specific surface area, fast ion-transport pathway and high power density. As an example, mesoporous carbon synthesized through carbonization of poly(vinyl alcohol) and inorganic salt mixture exhibited a specific capacitance of 180 F/g in aqueous H_2SO_4 electrolyte [74]. However, the volumetric specific capacitance, energy density and power density of mesoporous carbon electrodes could be influenced directly by the mesoporous size and content. A balanced population of mesopores and micropores is desirable for efficient electrochemical energy storage [75,76].

As discussed above, the size and shape of the pores in mesoporous carbon can be well controlled through various synthetic techniques [77]. When mesoporous carbon is produced as an ordered mesoporous carbon (OMC) with homogeneously distributed pores of regular size, it can facilitate charge storage and transport, and hence both the capacitance and rate capability can be improved. Highly OMCs with pore sizes of 2.8 nm (C-1) and 8 nm (C-2) have been synthesized using SBA-16 silica with mesostructured templates and polyfurfuryl alcohol as the carbon source [77]. The resultant OMCs, both C-1and C-2 with a specific surface area of 1880 and 1510 m^2/g, respectively, were tested as supercapacitor electrodes in different electrolytes. It was evident that the highest specific capacitance reached up to 205 F/g by the C-1 with a pore diameter of 2.8 nm whereas the C-2 with a pore diameter of 8 nm exhibited better stability while increasing the rate.

For mesoporous carbons, activation can also be performed to introduce micropores. For instance, Xia *et al.* activated mesoporous carbon with CO_2 at 950°C, which introduced micropores into the mesoporous carbon to improve the specific capacitance up to 223 F/g from 115 F/gin 6 M KOH [78]. The observed enhancement in specific capacitance can be attributable to the formation of hierarchical pores with a high specific surface area (2749 m^2/g) and the well-balanced populations of micropores and mesopores. Recently, production of mesoporous carbon through carbonization of non-conventional materials, like biomass, are becoming more and more popular. For example, N-doped mesoporous carbon has been prepared by a one-step method of pyrolysing the mixture of milk powder and potassium hydroxide without using any template. The N-doped mesoporous carbon (NMPC) showed a specific surface area of 2145.5 m^2/g and a pore volume of 1.25 cm^3/g. As a supercapacitor electrode material, the NMPC, with 2.5% N dopant, exhibited a specific capacitance of 396.5 F/g at 0.2 A/g in 6 M H_2SO_4 and stable capacitance retention of 95.9% after 2000 cycles at 50 mV/s [79]. Furthermore, the shape and

Table 1. Carbon nanomaterials in electrical double-layer capacitors (EDLCs).

Electrode	Electrolyte	Specific capacitance	Power density	Energy density	Retention capability	Ref.
(i) Carbon nanotube (CNT)						
CNT (functionalized by –OH and –COOH)	0.075 M Hydroquinone (HQ) into 1 M H_2SO_4 aqueous	3199 F/g at 5 mV/s	–	–	70% after 350 cycles	32
PEDOT/MWCNT	1 M $LiClO_4$	79 F/g	5000 W/kg	11.3 Wh/kg	85% after 1000 cycles	33
PTFE/PANI-CNT	30% KOH in H_2O	163 F/g at 0.1 A/g	–	–	–	34
C tubes	0.5 mol/l H_2SO_4	315 F/g at 0.35 V	–	–	–	37
SWNT	1 M Et_4NBF_4/ propylene carbonate	160 F/g at 4V	24 kW/kg	17 Wh/kg	96.4 after 1000 cycles	38
MWCNT	6 mol/l KOH	80–135 F/g	–	–	–	39
N-doped (8.64 wt. %) carbon shell and a CNT-core	6 mol/l KOH	205 F/g	–	–	97.1% after 1000 cycles	40
Spherical particles of N-doped CNT	1 M H_2SO_4	215 F/g at 0.2 A/g	–	–	99% after 1500 cycles	41
(ii) Graphene						
rGO	1-butyl-3-methylimidazolium hexafluorophosphate ($BMIPF_6$)	348F/g at 0.2 A/g current	–	–	120% after 3000 cycles at 10 mV/s	43
Graphene hydrogel	5 M KOH	220 F/g at 1 A/g current	30 kW/kg	5.7 Wh/kg	92% after 2000 cycles	44
rGO by Na_2CO_3	6 M KOH	228 F/g at 5 mA/cm^2	–	–	–	45
Graphene sheets	30 wt. % KOH in H_2O	150 F/g at 0.1 A/g current	–	–	100% up to 500 cycles	46
Exfoliated rGO	30 wt. % KOH in H_2O	264 F/g at 0.1 A/g current	–	–	97% after 100 cycles	47
MW assisted rGO	5 M KOH	191 F/g at 0.15 A/g current	–	–	9% reduction at 0.6 A/g	48
Hollow graphene	1-ethyl-3-methylimidazolium tetrafluoroborate/acetonitrile ($EMIMBF_4$/AN)	298 F/g at 1 A/g current	1000	35 Wh/kg		49
Exfoliated rGO	1-ethyl-3-methylimidazolium tetrafluoroborate/acetonitrile ($EMIMBF_4$/AN)	166 F/g at 5.7 A/g current and 3.5 V	250 kW/kg	70 Wh/kg	97% after 10 000 cycles	50
rGO (KOH activated)	Tetraethylammonium tetrafluoroborate (TEABF4) in acetonitrile	120 F/g	500 kW/kg	26 Wh/kg	95% after 2000 cycles	51

Table 1. *Continued.*

Electrode	Electrolyte	Specific capacitance	Power density	Energy density	Retention capability	Ref.
Graphene made porous carbon	1-ethyl-3-methylimidazolium bis(trifluoromethylsulfonyl) imide, [EMIM][TFSI] and Acetronitrile in 1:1 ratio	174 F/g at 4.1 A/g current	338 kW/kg	74 Wh/kg	94% after 1000 cycles	52
N-doped graphene	1 M tetraethylammoniumtetra-fluoroborate (TEA BF_4)	280 F/g at 20 A/g current in 6 M KOH	800 kW/kg	48 Wh/kg	99.8% after 230 000 cycles	53
N-doped (5.86 at.%) graphene hydrogel	6 M KOH	308 F/g at 3 A/g current	–	–	92% after 1200 cycles	54
3D N-doped graphene	1 M $LiClO_4$	484 F/g at 1 A/g and 415 at 100 A/g current	–	–	100% after 1000 cycles at 100 A/g current	55
B-doped rGO	6 M KOH solution	200 F/g at 0.1 A/g current	∼10 kW/kg	∼5.5 Wh/kg	95% after 4500 cycles	56
N/P doped rGO	6 M KOH solution	165 F/g at 0.1 A/g current			80% after 2000 cycles at 0.5 A/g	57
Graphene hydrogel (hydrothermal)	–	175 F/g at 10 mV/s	–	–	–	61
4.38% (at.) N-graphene hydrogel (hydrogel)	5 M KOH	131 F/g at 80 A/g current	144 kW/kg	4.5 Wh/kg	95.2% after 4000 cycles at 100 A/g	62
Graphene aerogel (3D printed)	3 M KOH	4.76 F/g at 0.4 A/g current	4.08 kW/kg	0.26 Wh/kg	∼95.5% after 10 000 cycles at 200 mV/s	69
Graphene aerogel	0.5 M H_2SO_4	325 F/g at 1 A/g	7 kW/kg	45 Wh/kg	∼98% after 5000 cycles	70
2D microporous covalent triazine-based framework	Solvent-free ionic liquid $EMIMBF_4$	151.3 F/g at 0.1 A/g current	10 kW/kg	∼42 Wh/kg	85% after 10 000 cycles at 10 A/g	71
(iii) Mesoporous carbon						
Porous carbon (Surface area (S_{BET}) = 1300 m^2/g, pore diameter (D_p) = 5–15 nm)	2 M H_2SO_4 1 M (C2H5)4NBF4 in acetonitrile	0.14 F/m^2 0.075 F/m^2(at 1 mA/cm^2)	2600 W/kg 4000 W/kg	1 Wh/kg 3 Wh/kg	85% at 100 mA/cm^2	74
Porous carbon (S_{BET} = 1600 m^2/g, D_p = 0.6–1.1 nm)	1.5 M (C2H5)4NBF4 in acetonitrile	100–140 F/g At 1 mA/cm^2	–	–	100% up to 100 mA/cm^2	75
Porous Carbon (S_{BET} = 1880 m^2/g, D_p = 2.8 nm)	6 M KOH	205 F/g at 1 mV/s	–	–	86.8% after 3000 cycles at 500 mA/g	77

Table 1. *Continued.*

Electrode	Electrolyte	Specific capacitance	Power density	Energy density	Retention capability	Ref.
Porous carbon (S_{BET} = 2749 m^2/g, D_p = 3–4 nm)	6 M KOH	223 F/g at 2 mV/s	–	–	73% at 50 mV/s	78
N-doped (2.5 at.%) mesoporous carbon (S_{BET} = 2145.5 m^2/g, D_p = 0.8–2.5 nm)	6 M H_2SO_4	396.5 F/g at 0.2 A/g current	–	–	95.9% after 2000 cycles at 50 mV/s	79
(iv) Hybrid carbon nanomaterials						
Graphene/carbon black	6 M KOH	175 F/g at 10 mV/s	–	–	98.9% after 6000 cycles (200 mV/s)	81
Porous carbon/rGO (S_{BET} = 1496 m^2/g, D_p = 1.4–3.5 nm)	6 M KOH	171 F/g at 10 mV/s scan	4.2 kW/kg	3.3 Wh/kg	74% at 0.1 A/g	82
rGO/CNT	0.1 M sodium phosphate buffered saline (PBS)	140 F/g at 0.1 A/g current	–	–	64.3% at 100 A/g	83
Graphene/CNT	1 M H_2SO_4	124 F/g at 0.1 V/s	–	–	95% at 1 V/s	85
Graphene/CNT fiber	Poly(vinyl alcohol) (PVA)/H_3PO_4 (1:1, mass)	31.5 F/g at 0.04 A/g	–	–	100% after 5000 cycles	86
SWNT/N-doped rGO fiber	PVA/H_3PO_4, 1 M H_2SO_4	300 F/g at 26.7 mA/cm^3, 305 F/g at 73.5 mA/cm^3	1085 mW/cm^3	6.3 Wh/cm^3	93% after 10 000 Cycles at 250 mA/cm^3	87
3D N-doped graphene/CNT	6 M KOH	180 F/g at 0.5 A/g current	–	–	96% after 3000 cycles	88
Freestanding graphene hydrogel/carbon fiber composite	1 M Na_2SO_4	150.2 F/g at 1 A/g current	–	–	97.9% after 2000 cycles	89

structure of pores of mesoporous carbon have also been explored to improve the electrochemical performance [80].

Hybrid carbon nanomaterials in EDLCs

Carbon nanomaterials with distinct structures can be combined to exhibit synergetic effects for electrochemical performance. For example, carbon black has been used to separate graphene sheets to produce 3D hybrid materials with minimized aggregation of graphene, leading to a high specific capacitance of 175 F/g at 10 mV/s scan rate in 6 M KOH electrolyte [81]. In other work, mesoporous carbon spheres were sandwiched between graphene sheets and the resulting 3D structure exhibited a specific capacitance of 171 F/g at the same 10 mV/s scan rate in 6 M KOH [82]. More interestingly, CNTs were intercalated between graphene sheets to retain the specific surface area of graphene by minimizing its aggregation [83]. The $\pi-\pi$ interaction between graphene and CNTs can also improve electrical conductivity and mechanical strength [84]. Just like GO to disperse CNTs in solvents [83], oxidized CNTs have been used to form composites with graphene [85]. In this context, Yu and Dai produced hybrid films of CNT and graphene interconnected network with well-defined nanoporous [85], which exhibited a specific capacitance of 120 F/g in 1 M H_2SO_4 electrolyte and an almost rectangular cyclic voltammogram even at a 1-V/s scan rate. Sun *et al.* reported other interesting work [86], in which graphene

sheets were intercalated between CNTs in aligned CNT fiber. Although the resultant hybrid fiber exhibited a specific capacitance of only 31.5 F/g, it was much higher than that of the pure CNT fiber (5.83 F/g). By using a modified hydrothermal microreactor, Yu *et al.* produced a continued CNT and graphene hybrid fiber with well-defined mesoporous structures [87], which showed a specific surface area as high as 396 m^2/g with an electrical conductivity of 102 S/cm. The corresponding fiber-shaped supercapacitor showed a volumetric specific capacitance of 305 F/cm^3 at 26.7 mA/cm^3 current density and a volumetric energy density of 6.3 mWh/cm^3, which is comparable to the energy density of a 4 V–0.5 mAh thin-film lithium-ion battery. Furthermore, a 3D N-doped CNT/graphene network was also synthesized through hydrothermal treatment and freeze-drying, followed by carbonizing GO and the pristine CNT mixture in the presence of pyrrole [88]. The resultant hybrid carbon fiber showed high electrochemical performance, especially capacitance retention of 96% after 3000 cycles [88]. In case of self-assembled carbon-composite material [89–94], freestanding 3D graphene hydrogel and carbon nanofiber composite material demonstrated 150.2 F/g specific capacitance at 1-A/g current with 97.8% capacitance retention after 2000 cycles [89]. Carbon nanofiber and nanotube network was also synthesized from conjugated polymer for electrochemical energy storage [90]. Table 1 summarizes carbon-based electrical double-layer supercapacitors (EDLCs).

Pseudocapacitors (PCs)

Pseudocapacitors store energy through reversible Faradaic charge transfer, which involves fast and reversible electrochemical redox reactions on the interface between the electrodes and electrolyte. As such, the specific capacitance of a pseudocapacitor is often higher than that of an EDLC, as is the energy density. As the redox reactions occur on the electrode surface, a high specific surface area and high electrical conductivity are essential for electrodes in a high-performance PC. Therefore, carbon nanomaterials, including CNTs, graphene, mesoporous carbon and their hybrids, have also been used as the substrate to load active materials and/or current collector to ensure high capacitance and fast charge transfer for electrodes in high-performance PCs.

CNTs in pseudocapacitors

CNTs have been used in pseudocapacitors in either a functionalized form or composited with other active components, such as conductive polymers and metal oxides. CNTs can be functionalized through chemical or electrochemical methods. The most common way to functionalize CNTs is acid oxidation (e.g. a mixture of concentrated sulfuric acid and nitric acid) to introduce surface carboxyl groups [95]. Through acid oxidation, the specific capacitance of CNTs can be increased by 3.2 times due to the increased hydrophilicity of the electrodes in aqueous electrolytes and the introduction of pseuducapacitance. Treatment of CNTs with NaOH solution at 80°C, followed by ultrasonication in H_2SO_4/HNO_3 solution, can also improve the specific capacitance from 28 F/g for the pristine CNTs to 85 F/g for the functionalized CNTs [32]. However, the oxidation treatments inevitably induced defects to degrade the CNT structure and reduce the electrical conductivity. Therefore, a delicate balance between the electrode performance and its structure integrity is important for high-performance pseudocapacitors (i.e. PCs).

Conducting polymers possessing good electrical conductivities and redox activities often exhibit high specific capacitances when they are composited with CNTs. In this regard, Bai *et al.* increased the energy density of a CNT-based PC by four times, up to 11.3 Wh/kg, by compositing poly (3,4-ethylenedioxythiophene) (PEDOT) homogenously onto the CNT electrode through in-situ polymerization [96]. Similarly, polypyrrole (PPy)/CNT composite electrodes have been also synthesized to yield a specific capacitance of 165 F/g in 1 M KCl solution [97]. Compared with PEDOT and PPy, PANI possesses a higher theoretical specific capacitance [98], which was confirmed by a high specific capacitance of 501.8 F/g reported for flexible PANI/SWNT composite films synthesized through in-situ electrochemical polymerization (Fig. 3) [99]. Subsequent electrodegradation further increased the specific capacitance to 706.7 F/g by forming charge transfer channels via selective dissolution of polycrystalline and off-lying disordered PANIs. Because PANI changes its color during the charge–discharge process, PANI/CNT composites have been used for high-performance (308.4 F/g in PVA/H_3PO_4) smart supercapacitors with highly reversible chromatic transitions during charge–discharge processes for monitoring the energy-storage status by the PANI color changes [100].

Metal oxides and hydroxides are two other important classes of active electrode materials for pseudocapacitors. Compared to conductive polymers, metal oxides and hydroxides often exhibit a better electrochemical stability but lower electrical conductivity. For metal oxides and hydroxides to

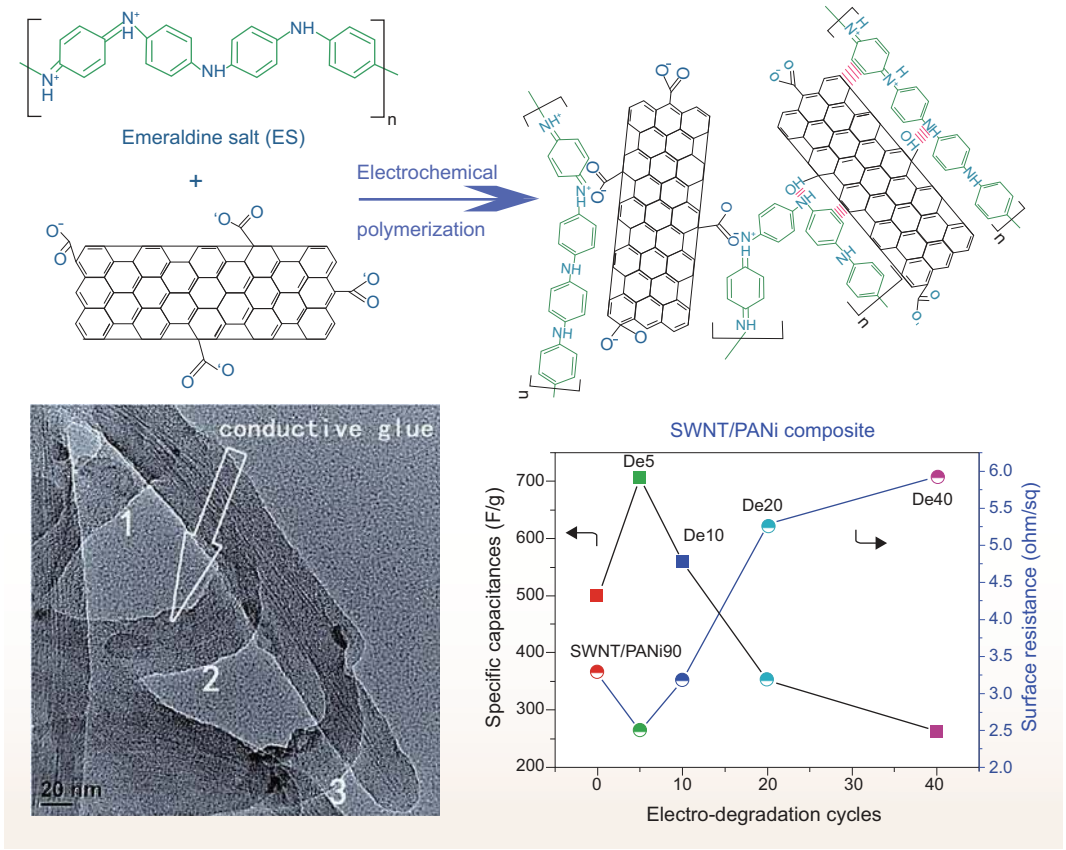

Figure 3. Schematic illustration and SEM image of PANI/SWNT composite for pseudocapacitor. Reproduced with permission from ref. [99]. Copyright of American Chemical Society (2010).

be used in high-performance pseudocapacitors, the corresponding metals must possess two or more oxidation states, which can coexist and inter-transfer freely. Examples include RuO_2, MnO_2, NiO, V_2O_5, Fe_2O_3, Co_3O_4, TiO_2, SnO_2, Mn_3O_4 and $Ni(OH)_2$ [101–108]. In the metal oxide and CNT composite electrodes, CNTs can not only provide the high electrical conductivity and large specific surface area for efficiently loading the active materials, but also effectively restrict the volumetric change of metal oxides or hydroxides caused by the cyclic charge–discharge processes [106]. As RuO_2 has three oxidation states and a wide operation potential window, RuO_2/CNTs have become a typical composite electrode material for pseudocapacitors. The specific capacitance of RuO_2 with a large surface area can reach up to 1170 F/g in 0.5 M H_2SO_4 electrolyte [108]. Reddy and Ramaprabhu have synthesized RuO_2/CNT, TiO_2/CNT, SnO_2/CNT composites by chemical reduction of corresponding salts to functionalize CNTs and demonstrated the highest capacitance of 160 F/g for the TiO_2/CNT [107]. On the other hand, MnO_2 possesses a high theoretical specific capacitance of 1370 F/g [109] and has been electrochemically deposited onto chemical vapor deposition (CVD)-grown CNT arrays to exhibit a specific capacitance of 642 F/g in 0.2 M Na_2SO_4 electrolyte [110]. Very high charge/discharge stability of up to 10 000 cycles can be obtained using MnO_2/CNT composite electrodes [111]. Furthermore, flexible and wearable supercapacitors based on MnO_2/CNT composite fibers prepared by electrochemical deposition of MnO_2 on aligned CNT fibers were demonstrated to show a specific capacitance of 3.707 mF/cm^2 [112].

Graphene in pseudocapacitors

Just like metal oxide and CNT electrodes, graphene with a high specific surface area and high electrical conductivity has also been composited with other active materials, including conductive polymers, metal oxides and hydroxides, as electrodes for pseudocapacitors [113–119]. Indeed, PANI/GO composites have been synthesized through in-situ polymerization of aniline into PANI on GO [113]. Depending on the mass ratio of PANI to GO, performance of the PANI/GO electrode varied and the highest specific capacitance of 746 F/g has been

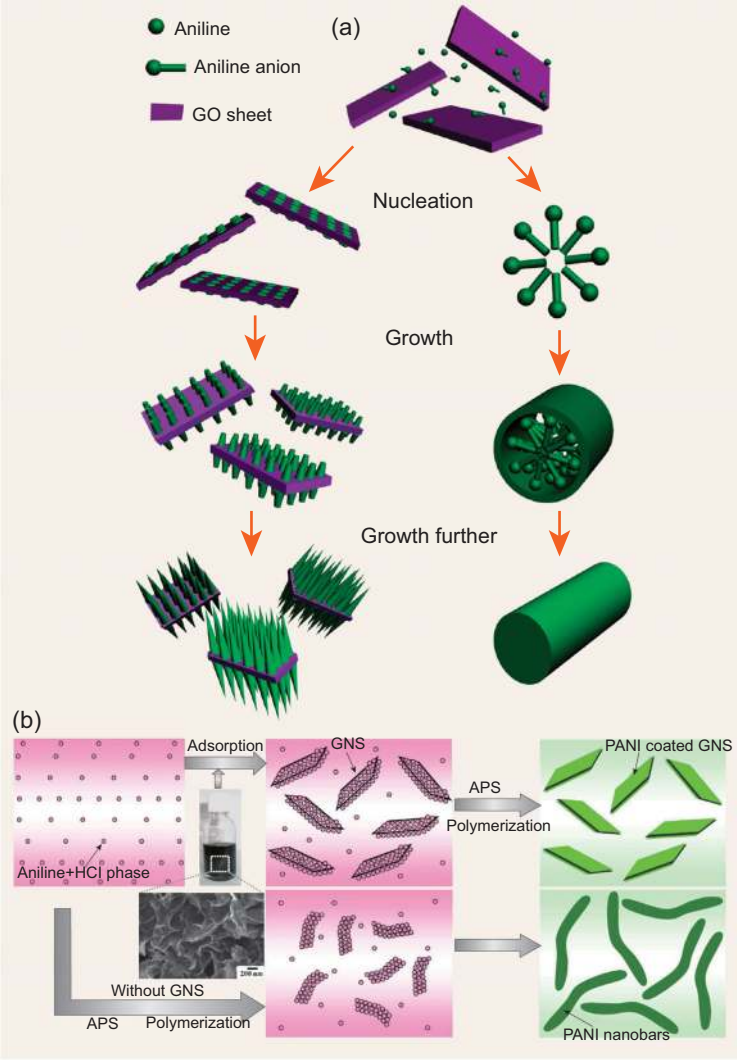

Figure 4. Schematic illustration to the heterogeneous nucleation on graphene oxide nanosheets and in bulk solution for the growth of PANI nanowires. Reproduced with permission from Ref. [114]. Copyright American Chemical Society (2010). (b) Schematic illustration for the synthesis of GNS/PANI composite. Reproduced with permission from Ref. [115]. Copyright of Elsevier (2010).

achieved at a PANI/GO mass ratio of 200/1. Like a pure PANI electrode, however, the PANI/GO composite electrode showed very poor electrochemical cyclic stability, with a retention rate of only 20% after 500 cycles. Increased electrochemical cyclic stability could be achieved by increasing the portion of GO in the PANI/GO composite and a 73% retention rate was obtained at the PANI/GO ratio of 23/1. By growing vertically aligned PANI nanowires on GO substrate (Fig. 4a) [114], the morphology of PANI and the mass ratio of PANI to GO can be well controlled to produce a specific capacitance as high as 555 F/g in 1 M H_2SO_4 at 0.2 A/g with a 92% retention rate after 2000 cycles at 1 A/g. Yan *et al.* also synthesized a PANI/graphene composite with PANI nanoparticles (2 nm) uniformly decorated on the graphene flakes (Fig. 4b) [115]. In this work, graphene not only acted as a support material to offer active sites for the nucleation of PANI, but also provided a better electron-transfer path, leading to a specific capacitance of 1046 F/g in 6 M KOH at a 1-mV/s scan rate, energy density of 39 Wh/kg and power density of 70 kW/kg. To further improve the performance, graphene sheets with more active nucleation sites were prepared by unzipping CNTs to produce graphene nanoribbons with a specific capacitance of 340 F/g and a retention rate of 90% after 4200 charge–discharge cycles [116]. More interestingly, an even higher specific capacitance of 989 F/g in 6 M KOH electrolyte was obtained when cobalt was introduced into PANI/graphene composites through polymerizing aniline in the presence of both cobalt and graphene [117].

3D PANI/graphene composite hydrogel was also synthesized as a freestanding film to prepare flexible supercapacitors without binders [118,119], which exhibited excellent energy-storage properties as well as outstanding flexibilities for portable electronic devices. More recently, a simple and cost-effective method was reported to produce graphene/polystyrene sulfonic acid-graft-aniline (Gr/S-g-A) nanocomposite through direct exfoliation of graphite using S-g-A as a surfactant [120]. The Gr/S-g-A composite electrode was demonstrated to exhibit a superior specific capacitance of 767 F/g at 0.5 A/g current density in 0.1 M Bu_4NPF_6/acetonitrile electrolyte with 92% capacitance retention after 5000 cycles. The corresponding supercapacitor showed an energy density of 208.8 Wh/kg and a power density of 347.8 W/kg [120].

In addition to PANI, polypyrrole (PPy) has also been composited with graphene simply by directly mixing PPy with RGO [121]. The PPy/graphene composite thus produced showed a specific capacitance of 400 F/g in 2 M H_2SO_4 at a current density of 0.3 A/g. PPy/GO composite was also synthesized through in-situ chemically polymerizing pyrrole monomers in the presence of $FeCl_3$ to improve uniformity of the composite, and hence a slightly improved specific capacitance of 421.42 F/g in 0.1 M KCl electrolyte [122]. By substituting $FeCl_3$ with ammonium persulfate dissolved in citric acid, the specific capacitance was further improved to 728 F/g at 0.5 A/g current density with a retention rate of 93% after 1000 cycles [123]. Similarly to PANI, PPy can also be assembled with GO into layer-by-layer composites through the electrostatic interaction [124]. However, the electrochemical performance of PPy/GO composite is not promising due to the poor electrical property of GO.

Through electrochemical polymerization of pyrrole monomer and simultaneous electrostatic deposition, Zhao *et al*. also synthesized 3D PPy/graphene composites [125]. The resulting 3D PPy/graphene composite foam exhibited a specific capacitance of 350 F/g at a current density of 1.5 A/g with no change in the initial capacitance even after 1000 cycles. In another attempt, PPy/graphene composite films were prepared through electrochemical polymerization of PPy on graphene pre-deposited electrophoretically onto a Ti substrate [126], leading to a specific capacitance of 1510 F/g (or 151 mF/cm^2, or 151 F/cm^3) in 0.1 M $LiClO_4$ electrolyte at the 10-mV/s scan rate. This ultrahigh specific capacitance was attributed to the porous structure, effective utilization of the pores and the large specific surface area for rapid redox reactions during the charge–discharge process in the pseudocapacitor.

As is the case for CNTs, metal oxides or hydroxides can also be composited with graphene-based nanomaterials to improve the pseudocapacitance. In this context, MnO_2/GO composite with MnO_2 nanoneedles deposited on the GO was synthesized through the chemical reaction of $KMnO_4$ and $MnCl_2$ in water/isopropyl alcohol mixture in the presence of GO [127]. The as-synthesized MnO_2/GO composite exhibited a specific capacitance of 216 F/g and a retention of 84.1% after 1000 cycles. By perpendicularly grafting polymer brushes, poly(sodium methacrylic acid), onto the GO sheets prior to loading of MnO_2 nanoparticles, MnO_2/GO composite with uniformly distributed MnO_2 on the GO substrate was prepared, which showed an improved specific capacitance of 372 F/g in 1 M Li_2SO_4 at 0.5A/g current density and an increased retention rate of 92% after 4000 cycles [128]. Alternatively, MnO_2/GO composite with porous structure has also been synthesized with the aid of microwave irradiation [129,130] to exhibit a specific capacitance of 310 F/g at a 2-mV/s scan rate and 228 F/g at a high scan rate of 500 mV/s. Besides, Mn_3O_4/graphene composite was also prepared to show a specific capacitance of 271.5 F/g at 0.1 A/g and 180 F/g at even a high current density of 10 A/g with no obvious decay of capacitance even after 20 000 cycles [131]. A filtration technique was also developed for preparing freestanding Mn_3O_4/graphene composite film as the electrode [132]. With regard to carbon-supported metal oxide PCs, Vanadium phosphates ($VOPO_4$)/graphene composited with vertically aligned porous 3D structure obtained through an ice-templated self-assembly process showed a 527.9-F/g gravimetric capacitance at 0.5-A/g current density with 85% capacitance retention after 5000 cycles at a 100-mV/s scan rate in 6 M KOH electrolyte—promising supercapacitive performance [133].

RuO_2, a highly active metal oxide for redox reactions, has also been composited with graphene as electrodes in pseudocapacitors. RuO_2/graphene composite was synthesized most commonly through a sol-gel technique, followed by annealing, to exhibit a specific capacitance of 570 F/g in 1 M H_2SO_4 and a retention rate of 97.9% after 1000 cycles [134]. This method could effectively reduce the aggregation of both RuO_2 nanoparticles and graphene sheets by separating graphene sheets with the grafted RuO_2 nanoparticles. An energy density up to 20.1 Wh/kg at 0.1-A/g current density was achieved, which remained at 4.3 Wh/kg when the power density approached 10 kW/kg.

Cobalt oxide is another kind of metal oxide that can demonstrate rapid and reversible redox reactions during the charge–discharge process in pseudocapacitors. For example, Co_3O_4/graphene composite was synthesized via a chemical reaction of cobalt nitrate with urea in GO suspension under microwave irradiation to exhibit a specific capacitance of 243.2 F/g in 6 M KOH [135]. Co_3O_4/graphene composite can also be synthesized by a hydrothermal method, followed by calcination to improve the electrochemical performance [136]. Morphology of the resultant Co_3O_4/graphene composite depends strongly on the ratio of Co_3O_4 to graphene. At a 7% mass ratio of graphene, Co_3O_4 nanoplates homogeneously grew on the graphene sheets, leading to improved specific capacitances of 667.9 and 385.1 F/g at the current densities of 1.25 and 12.5 A/g, respectively. Besides,Co_3O_4 and $Co(OH)_2$ could also be composited with graphene to prepare pseudocapacitor electrodes. In particular, a sheet-on-sheet-structured $Co(OH)_2$/graphene composite was synthesized through a one-step in-situ hydrothermal method to exhibit a specific capacitance of 540 F/g at a high current density of 10 A/g [137]. Increased specific capacitances with charge–discharge cycles were observed for both the Co_3O_4/graphene and $Co(OH)_2$/graphene composites, attributable to a gradual activation of the active materials wrapped up by graphene during the initial charge–discharge cycling [136].

Apart from Mn, Ru and Co oxides, oxides of other metals with multiple valences, such as Ni, Fe, Ti and Zn, have also been under research focus as alternative electrode materials that can be composited with graphene to further improve pseudocapacitive performance [138–142]. For instance, hexagonal nanoplates of single-crystal $Ni(OH)_2$ have been grown on lightly oxidized conductive graphene sheets using an in-situ synthesis technique [138]. The resultant composite exhibited an

ultrahigh specific capacitance of 1335 F/g in 1 M KOH at a current density of 2.8 A/g with a remarkably high-rate capability of 953 F/g at 45.7 A/g and an excellent cycling stability (94.3% specific capacitance retained after 3000 cycles).

Self-assembled graphene-based structures, such as hydrogels and aerogels, were also extensively utilized for pseudocapacitor electrode applications [143]. In particular, Zhang *et al.* recently developed a plasma treatment approach to fabricate 3D N-doped graphene aerogel/Fe_3O_4 nanostructures, which showed a specific capacitance of 386 F/g in 6 M KOH electrolyte with a 97% retention rate after 1000 cycles [144]. In-situ growth of active materials on a graphene substrate can achieve high energy-storage properties because of the intimate interactions and efficient charge transfer between active nanomaterials and the conductive graphene substrate. Among other self-assembled graphene-based 3D structures, graphene hydrogels modified with different oxygen-containing groups using hydroquinones [145], MnO_2/graphene hydrogel composites [146,147], graphene hydrogels modified with 2-aminoanthraquinone [148], RuO_2/reduced graphene-oxide hydrogels [149], freestanding polyaniline/reduced graphene-oxide composite hydrogels [150] and single-crystalline Fe_2O_3 nanoparticles directly grown on graphene hydrogels [151] have been studied. Details of their supercapacitive performance have been summarized in Table 2. Self-assembled porous graphene networks synthesized from various organic chemicals have also been used for supercapacitor applications. These structures are generally called organogels [152–155]. However, more studies are needed for better understanding the mechanism of charge storage in such organogels for improving their performance as efficient supercapacitor electrodes.

Similarly to EDLCs, it is highly desirable to improve the volumetric capacitance of graphene-based PCs for practical applications. In this context, Xu *et al.* recently reported a PC fabricated using a PANI and graphene composite monolith, which demonstrated 802 F/cm^3 volumetric capacitance at 54% PANI loading and 66% of the capacitance was maintained when the current density increased by 100 times [156].

Mesoporous carbon in pseudocapacitors

Mesoporous carbon with functional groups can act as efficient pseudocapacitor electrodes. The use of strong activation reagents, such as sulfuric acid, nitric acid and ammonium persulfate, to activate mesoporous carbons can not only introduce micropores, but also introduce various functional groups with additional pseudocapacitance. For example, OMC activated by nitric acid possesses small-sized mesopores as well as functional groups, including −OH, −COOH and/or −C=O, and showed improvement in specific capacitance from 117 to 295 F/g at a 10-mV/s scan rate in aqueous alkali electrolyte [157]. By pyrolysing the iron fumarate metal organic frameworks, Wang *et al.* recently adopted a simple and scalable technique to synthesize porous carbon nanorods (Fe_3O_4-DCN) supported by 3D kenaf stem-derived macroporous carbon (KSPC) for high-performance supercapacitors [158]. The 3D-KSPC/Fe_3O_4-DCN was employed as an efficient electrode in supercapacitors to exhibit a high specific capacitance of 285.4 F/g in 2 M KOH at 1-A/g current density with the capacitance remaining at 220.5 F/g even after 5000 cycles at 2 A/g. Mesoporous carbon has also been composited with other active materials, including conductive polymers and metal oxides, as electrode materials in pseudocapacitors, as exemplified by PANI nanowires grown onto ordered bimodal mesoporous carbon via chemical polymerization [159]. The resultant PANI/mesoporous carbon composite exhibited a specific capacitance of 517 F/g in 1 M H_2SO_4 and a retention rate of 91.5% after 1000 cycles due to the combination of the outstanding electrochemical properties of PANI and hierarchical porous structures of mesoporous carbon.

In the case of N-doped carbon (NC), previous studies suggested that four different types of nitrogen (pyrrolic N, pyridinic N, quaternary N/graphitic N and N oxides of pyridinic N) can be introduced into NCs, depending on the heat-treatment temperature and nitrogen sources [160,161]. Since conventional synthetic methods cannot produce NC with a single N component (e.g. pyrrolic N, pyridinic N or quaternary N/graphitic N), it is very difficult to determine the real role of different N-functional groups. NCs are reported to demonstrate not only double-layer capacitance, but also pseudocapacitance [51,162]. The mechanism of pseudocapacitance in NCs has yet been confirmed, although some preliminary studies have indicated that the presence of nitrogen atoms on the edges of graphene sheets (e.g. pyridinic N) played a crucial role [160].

Hybrid carbon nanomaterials in pseudocapacitors

As mentioned earlier, different carbon nanomaterials can be combined together to exhibit a synergetic effect. For pseudocapacitors, CNT and graphene have also been composited with PANI via in-situ polymerization [163]. The resultant

Table 2. Carbon nanomaterials in pseudocapacitors (PCs).

Electrode	Electrolyte	Specific capacitance	Power density	Energy density	Retention capability	Ref.
(i) Carbon nanotube (CNT)						
Poly(3,4-ethylenedioxythiophene) or PEDOT/MWCNT	1 M $LiClO_4$	79 F/g at 1 A/g current	5 kW/kg	11.3 Wh/kg	85% after 1000 cycles	96
Polypyrrole-coated MWCNT	1 M KCl	165 F/g at 0.5 mA/cm^2 current	–	–	100% after 1000 cycles	97
Polyaniline (PANI)/SWNT	0.5 M H_2SO_4	706.7 F/g at 5 mV/s	–	–	–	99
PANI/aligned CNT	PVA/H_3PO_4 (1:0.85, mass)	308.4 F/g at	–	–	73.9%	100
RuO_2/MWCNT, TiO_2/MWCNT, SnO_2/MWCNT	1 M H_2SO_4	138 F/g, 160 F/g, 93 F/g at 2 mV/s	500 W/kg	36.8, 40.2, 25 Wh/kg	–	107
RuO_2/CNT	0.5 M H_2SO_4	1170 F/g at 10 mV/s	–	–	82% at 400 mV/s	108
MnO_2/CNT	0.2 M Na_2SO_4	642 F/g at 10 mV/s	–	–	100% up to 700 cycles	111
MnO_2/CNT	1 M Na_2SO_4	201 F/g at 1 A/g current	600 W/kg	13.3 Wh/kg	100% up to 10 000 cycles at 1 A/g	112
(ii) Graphene						
GO-doped polyaniline (PANI)	1 M H_2SO_4	531 F/g at 0.2 A/g current	–	–	–	113
PANI nanowire/GO	1 M H_2SO_4	555 F/g at 0.2 A/g current	–	–	92% after 2000 cycles at 1 A/g	114
Graphene sheet/PANI	6 M KOH	1046 F/g at 1 mV/s	70 kW/kg	39 Wh/kg	–	115
PANI nanorods/graphene nanoribbon	1 M H_2SO_4	340 F/g	3.15 kW/kg, 9.47 kW/kg	7.56 Wh/kg, 4.01 Wh/kg	90% after 4200 cycles	116
Co-PANI/graphene	6 M KOH	989 F/g at 2 mV/s	1.581 kW/kg	352 Wh/kg	79% after 1000 cycles	117
3D graphene/PANI hydrogel	6 M KOH	334 F/g at 3 A/g current	–	–	57% after 5000 cycles	118
PANI/graphene	1 M H_2SO_4	375.2 F/g at 0.5 A/g current	1 kW/kg	30.34 Wh/kg	90.7% after 500 cycles at 3 A/g	119
Graphene/poly(styrenesulfonic acid-graft-aniline)	0.1 M Bu_4NPF_6/acetonitrile	767 F/g at 0.5 A/g current	0.35 kW/kg	208.8 Wh/kg	92% after 5000 cycles	120
Graphene/polypyrrole (PPy) nananotubes	2 M H_2SO_4	400 F/g at 0.3 A/g current	–	–	88% after 200 cycles at 1.5 A/g	121

Table 2. *Continued.*

Electrode	Electrolyte	Specific capacitance	Power density	Energy density	Retention capability	Ref.
PPy/GO	0.1 M KCl	421.4 F/g at 2 mA current	–	–	–	122
Graphene/PPy nanowires	1 M KCl	728 F/g at 0.5 A/g current	–	–	93% after 1000 cycles	123
Pillared GO/PPy	2 M H_2SO_4	510 F/g at 0.3 A/g current	–	–	70% after 1000 cycles at 5A/g	124
PPy/3D graphene foam	3 M $NaClO_4$	350 F/g at 1.5 A/g current	–	–	100% after 1000 cycles	125
PPy/Graphene	0.1 M $LiClO_4$	1510 F/g at 10 mV/s	3 kW/kg	5.7 Wh/kg	Stable up to 25 cycles	126
GO/MnO_2 needles	1 M Na_2SO_4	216 F/g at 0.15 A/g current	–	–	84.1% after 1000 cycles at 0.2 A/g	127
Amorphous MnO_2/GO	1 M Li_2SO_4	372 F/g at 0.5 A/g current	–	–	92% after 4000 cycles at 0.5 A/g	128
MnO_2/porous graphene	1 M H_2SO_4	256 F/g at 0.25A/g current	24.5 kW/kg	20.8 Wh/kg	87.7% after 1000 cycles	129
MnO_2/graphene	1 M Na_2SO_4	310 F/g at 2 mV/s	–	–	88% at 100 mV/s	130
Mn_3O_4/graphene sheets	6 M KOH	271.5 F/g at 0.1 A/g current	–	–	100% after 20 000 cycles	131
Mn_3O_4/graphene paper	Potassium polyacrylate (PAAK)/KCl	321.5 F/g at 0.5 A/g current	–	–	–	132
3D $VOPO_4$/graphene	6 M KOH	527.9 F/g at 0.5 A/g current	–	–	85% after 5000 cycles at 100 mV/s	133
RuO_2/Graphene sheets	1 M H_2SO_4	570 F/g at 1 mV/s	10 kW/kg	20.1 Wh/kg	97.9% after 1000 cycles at 1 A/g	134
Co_3O_4/graphene sheets	6 M KOH	243.2 F/g at 10 mV/s	–	–	95.6% after 2000 cycles at 200 mV/s	135
Co_3O_4 nanoplates/graphene sheets	2 M KOH	667.9 F/g at 1.25 A/g current	–	–	81.3% after 1000 cycles	136
$Co(OH)_2$/graphene sheet layers	1 M KOH	622 F/g at 2 A/g current	15.8 kW/kg	86.6 Wh/kg	80% after 10 000 cycles at 10 A/g	139
$Ni(OH)_2$/graphene	1 M KOH	1335 F/g at 2.8 A/g current	10 kW/kg	37 Wh/kg	100% after 2000 cycles at 28.6 A/g.	140

Table 2. *Continued.*

Electrode	Electrolyte	Specific capacitance	Power density	Energy density	Retention capability	Ref.
α-Fe_2O_3 nanotubes/rGO	0.1 M K_2SO_4	181 F/g at 3A/g current	–	–	108% after 2000 cycles at 5A/g	141
TiO_2/graphene	1 M KOH	84 F/g at 10 mV/s	–	–	87.5% after 1000 cycles at 2 A/g	142
ZnO/graphene	1 M KOH	62.2 F/g	8.1 kW/kg	–	94.9% after 200 cycles	143
Fe_3O_4/N-doped graphene aerogel	6 M KOH	386 F/g at 5 mV/s	–	–	153% after 1000 cycles	144
Graphene hydrogel functionalized using hydroquinones	1 M H_2SO_4	441 F/g at 1 A/g current	–	–	86% after 10 000 cycles at 10 A/g	145
MnO_2/graphene hydrogel	1 M KOH	445.7 F/g at 0.5 A/g current	6.4 kW/kg	∼18 Wh/kg	82.4% after 5000 cycles at 50 mV/s	146
MnO_2/rGO hydrogel and aerogel	1 M Na_2SO_4	242 and 131 F/g at 1 A/g current	0.82 kW/kg	212 Wh/kg	89.6% after 1000 cycles	147
Graphene hydrogel modified by 2-aminoanthraquinone	1 M H_2SO_4	258 F/g at 0.3 A/g current			Slightly increased after 2000 cycles at 10 A/g	148
15% RuO_2/rGO hydrogel	1 M H_2SO_4	345 F/g at 1 A/g current	–	–	100% after 2000 cycles at 1 A/g	149
PANI/graphene hydrogel	1 M H_2SO_4 and 1 M H_2SO_4 + 0.4 M Hydroquinone	223.82 and 580.52 F/g at 0.4 A/g current	2.637 kW/l	13.2 Wh/l	87.5 and 70% after 5000 cycles at 10 A/g	150
Single-crystal Fe_3O_4/graphene hydrogel	1 M KOH	908 F/g at 2 A/g current	–	–	69% at 50 A/g	151
Graphene organogel	1 M propylene carbonate in tetraethylammonium tetrafluoroborate	140 F/g at 1 A/g	16.3 kW/kg	15.4 Wh/kg	64.3% at 30 A/g	152
Polyethyleneimine-induced coagulated graphene-oxide nanosheets from the dispersion	6 M KOH	46.3 mF/cm^2 at 0.1 A/g	–	–	98% after 1000 cycles at 10 A/g	153
(iii) Mesoporous carbon						
Oxygen/porous carbon (S_{BET} = 578 m^2/g, D_p = 2.2, 5.3 nm)	6 M KOH	295 F/g at 10 mV/s	–	–	100% after 500 cycles at 10 mV/s	157
Fe_3O_4/porous carbon nanorods (S_{BET} = 25.7 m^2/g, D_p = 14.9 nm)	2 M KOH	285.4 F/g at 1 A/g current	–	–	104% after 5000 cycles at 2 A/g	158
PANI nanowire/porous carbon (S_{BET} = 599 m^2/g, D_p = 2.4, 5 nm)	1 M H_2SO_4	517 F/g at 0.1 A/g current	–	–	91.5% after 1000 cycles at 0.5 A/g	159

Table 2. *Continued.*

Electrode	Electrolyte	Specific capacitance	Power density	Energy density	Retention capability	Ref.
(iv) Hybrid carbon nanomaterial						
Graphene sheet/CNT/PANI	6 M KOH	1035 F/g at 1 mV/s scan	–	–	94% after 1000 cycles at 200 mV/s	163
N-doped porous carbon/MWCNT (S_{BET} = 1270 m^2/g, D_p = 2.8 nm)	1 M H_2SO_4	262 F/g at 0.5 A/g current	–	–	–	164
PANI-graphene/CNT	1 M KCl	271 F/g at 0.3 A/g current	2.7 kW/kg	188.4 Wh/kg	82% after 1000 cycles at 2 A/g	165
Graphene-MnO_2/CNT	1 M Na_2SO_4/ polyvinylpyrrolidone (PVP)	486.6 F/g at 1 A/g current	∼ 1.7 kW/kg	15 Wh/kg	92.8% after 800 cycles at 1 A/g	166
Cobalt chloride carbonate hydroxide nanowire/AC	1 M KOH	1737 F/g at 2.5 mA/cm^2 current	0.1 kW/kg	29.03 Wh/kg	85.6% after 1000 cycles at 7.5 mA/cm^2	168
Patronite (VS_4)/SWNT/rGO	0.5 M K_2SO_4	558.7 F/g at 1 A/g current	13.85 kW/kg	174.6 Wh/kg	97% after 1000 cycles	169
PANI/GO/graphene	2 M H_2SO_4	793.7 F/g at 1A/g current	2.14 kW/kg	50.2 Wh/kg	80% after 1000 cycles at 100 mV/s	170
$Ni(OH)_2$-graphene/CNT stacked layers	2 M KOH	1065 F/g at 22.1 A/g current	8 kW/kg	35 Wh/kg	96% after 20 000 cycles at 21.5 A/g	171

PANI/CNT/graphene composite showed a specific capacitance as high as 1035 F/g in 6 M KOH electrolyte at a 1-mV/s scan rate, which is comparable with that of PANI/graphene (1046 F/g) and higher than that of PANI/CNT (780 F/g) or pure PANI (780 F/g). Moreover, 94% of the initial capacitance was maintained after 1000 cycles, though the corresponding retention rates for the PANI/graphene and PANI/CNT composites were only about 52% and 67%, respectively. Similarly, various efforts have also been made to explore other ternary composites (e.g. metal oxide/CNT/graphene, conductive polymer/metal oxide/graphene, N-doped microporous carbon/CNT) [164–167]. Of particular interest, cobalt chloride carbonate hydroxide nanowire arrays (CCCH NWAs) with an average length of 8 mm were synthesized on a Ni foam surface via a simple hydrothermal process to show a specific capacitance as high as 1737 F/g in 1 M KOH at 2.5 mA/cm^2, and angood cycling stability with a capacitance retention of 87.3% after 2000 cycles at a current density of 7.5 mA/cm^2. An asymmetric supercapacitor based on CCCH NWAs as positive and activated carbon as negative electrodes exhibited an energy density of 29.1 Wh/kg and a power density of 100 W/kg with a good stability over a wide voltage rang of 0–1.6 V [168]. Patronite (VS_4) has also been demonstrated to perform well in combination with SWNT and rGO to show a specific capacitance of 558.7 F/g in 0.5 M K_2SO_4 at 1-A/g current density in 0.5 M K_2SO_4 electrolyte and to deliver an energy density of 174.6 Wh/kg with a power density of 13.85 kW/kg [169]. Recently, the combination of both GO and pristine graphene with PANI has led to a specific capacitance of 793.7 F/g in 2 M H_2SO_4 at a 1-A/g current density [170]. This symmetric supercapacitor has exhibited an energy density of 50.2 Wh/kg at a power density of 2.14 kW/kg, attributable to the synergistic effects of the individual ingredient. A graphene and CNT stacked structure has also been conceived for supercapacitor applications [171,172]. Table 2 summarizes carbon-based pseudocapacitors.

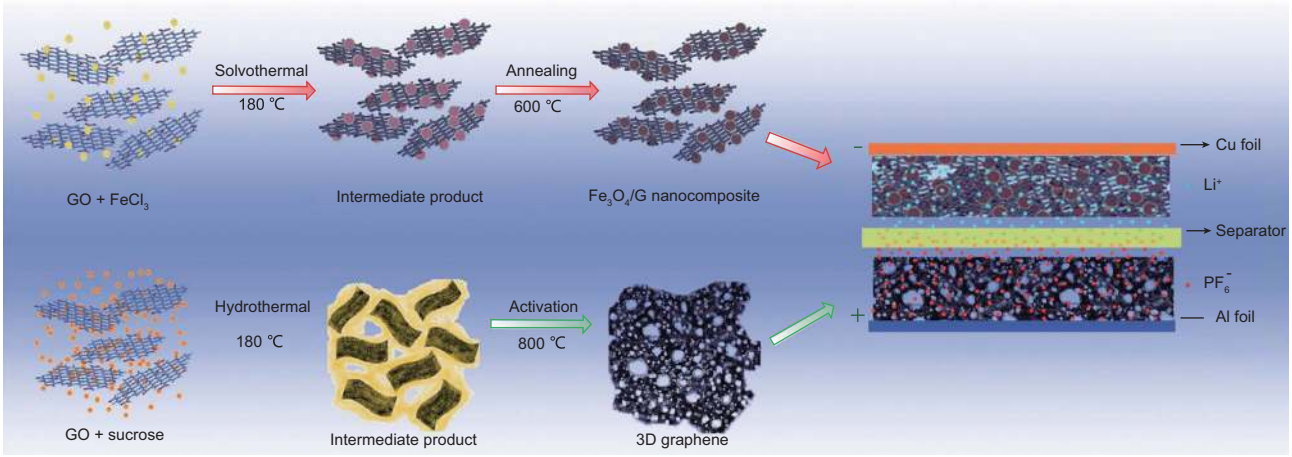

Figure 5. Schematic illustration of the synthesis of the negative electrode material Fe_3O_4/G nanocomposite and the positive electrode material 3D graphene, together for the configuration of a Li-ion containing organic hybrid supercapacitor. Reproduced with permission from ref. [179]. Copyright of The Royal Society of Chemistry (2013).

Carbon-based hybrid supercapacitors

Hybrid supercapacitors (HSCs) are mainly introduced to bridge the gap between ESCs that have high power but low energy and batteries that have high energy but low power. Actually, in most cases, HSC consists of a capacitive carbon electrode matched with either a peseudocapacitive or a lithium-insertion electrode (Fig. 1) [173–176]. In HSCs, the combination of the Faradaic intercalation on cathode and non-Faradaic surface reaction on anode (Fig. 1c) provides an opportunity to achieve both high energy and power densities even without compromising the cycling stability and affordability.

The reported carbon-based electrodes so far used for the cathode in HSCs are graphite, CNTs, graphene, activated carbon (AC), 3D mesoporous carbons and different metal oxide or polymer-based carbon composites [177]. 3D graphene/MnO_2 composite has a maximum specific capacitance of 1145 F/g, which is about 83% of the theoretical capacitance at a mass loading of 13% of MnO_2 [178]. On the other hand, HSCs were fabricated using a Fe_3O_4 nanoparticle/graphene composite by a simple solvothermal method (Fig. 5). Fe_3O_4/graphene-based half-cell exhibited a high reversible specific capacity exceeding 1000 mAh/g at a current density of 90 mA/g with an excellent rate of capability and cycle stability [179]. When this composite was assembled in a Li-ion-based ($LiPF_6$) HSC, energy densities of 204–65 Wh/kg and power densities from 55 to 4600 W/kg were achieved [179]. Besides, Lim *et al.* reported HSCs based on a mesoporous Nb_2O_5/carbon-composite anode and AC (MSP-20) cathode, showing excellent energy and power densities of 74 Wh/kg and 18 510 W/kg (at 15 Wh/kg), respectively, with a capacity retention rate of 90% at 1000 mA/g after 1000 cycles in the mixture electrolyte of LiPF6 (1.0 M)/ethylene carbonate and dimethyl carbonate (1:1 volume ratio) [180]. Li *et al.* reported a hybrid-type supercapacitor based on N-doped AC, which showed high material-level energy densities of 230 Wh/kg with a power density of 1747 W/kg and a capacity retention of 76.3% after 8000 cycles [181].

Carbon-based bendable supercapacitors (film-/fiber-shaped)

Along with the recent development of flexible and wearable electronics, flexible and wearable SCs, in either a thin film or fiber-shaped (coating, fabric/cloth, paper, textile, etc.), have attracted increasing attention as advanced power sources. Due to their large surface area, excellent mechanical and electrical properties, and high electrochemical stability, carbon nanomaterials are also promising as electrode materials for flexible supercapacitors (FSCs). In this context, Chen *et al.* produced flexible and transparent supercapacitors based on In_2O_3 nanowire/CNT heterogeneous films, and observed an increase in specific capacitance up to 64 F/g with increasing numbers of In_2O_3 nanowires (up to 0.007 mg) dispersed on the CNT films [182]. In another study, a 2-mm-thick film-based FSC made of MnO_2 nanosheet-decorated carbon nanofiber electrodes was demonstrated to show a gravimetric capacitance of 142 F/g at a slow scan rate (~10 mV/s) when the electrode was interfaced with PVA-$H_4SiW_{12}O_{40}$·nH_2O [183]. Other materials used for the electrode in FSCs include TiO_2/MWNT/PEDOT composited carbon fibers [184] and various carbon papers made of fibers,

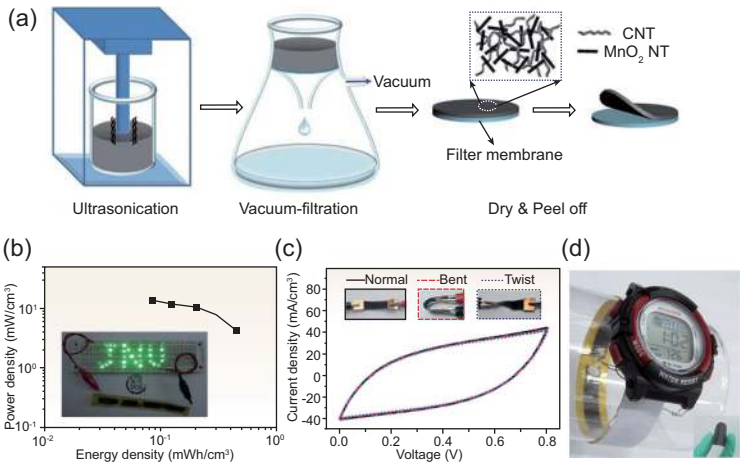

Figure 6. (a) Schematic illustration of the fabrication process of flexible freestanding CNT/MnO_2 NT hybrid film. (b) Ragone plots of the flexible solid-state SC device. Inset shows a group of LEDs (consisting of 32 green LEDs) powered by four series-connected SCs. (c) CV curves collected at the same scan rate of 5 mV/s under normal, bent and twisted conditions; insets are the digital images under the corresponding test conditions. (d) An electronic watch wrapped around a transparent glass tube demonstrating the flexibility of the SC-integrated watch band. Reproduced with permission from ref. [187]. Copyright of The Royal Society of Chemistry (2014).

aerogel and nanotubes [185]. Liu *et al.* fabricated highly flexible porous films of carbon nanofibers (P-CNFs) by an electro-spinning technique combined with a Co ion-assistant acid corrosion process [186]. The resultant fibers have high conductivity and outstanding mechanical flexibility, with little change in their resistance under repeated bending many times, even upto 180°. The P-CNF electrode showed a specific capacitance of 104.5 F/g in 0.5 M H_2SO_4 at 0.2 A/g current, effectively improved cycling stability and 94% retention of specific capacitance after 2000 charging/discharging cycles, along with a retention rate of 89.4% capacitance after 500 bending cycles [186]. These remarkable performances are attributable to the high graphitization degree and the unique hierarchical pore structures of P-CNF [186].

A low processing cost for flexible electrode manufacturing is always desirable. Du *et al.* developed a low-cost, flexible and high-performance hybrid electrode based on a MnO_2 nanotube (NT) and CNT composite film obtained through a vacuum-filtering method [187]. Due to the ultra-long 1D nanotube morphology, the synergetic effects between pseudocapacitive MnO_2-NTs and conductive CNTs, the hierarchical porous structure of the freestanding film and the high mass loading of MnO_2 (4 mg/cm^2), the resultant MnO_2-NT/CNT electrodes showed excellent mechanical and electrochemical performance with a volumetric capacitance of 5.1 F/cm^3 in the polyvinyl alcohol (PVA)/LiCl gel electrolyte, a high energy density of 0.45 mWh/cm^3 for the entire FSC volume and the retention of capacitance at about 105% of the initial capacitance after 6000 cycles due to a self-activation effect. As shown in Fig. 6, these SCs can be integrated in wearable electronic devices as flexible power that can drive watches and light emitting diodes (LEDs).

Flexible supercapacitors have also been fabricated from conducting polymers with and without compositing with other electrode materials (e.g. CNTs, graphene). PANI, PPy and PEDOT possess high specific capacitances of 1284, 480 and 210 F/g, respectively [188]. PPy is a popular polymer electrode material for FSCs due to its high environmental stability, excellent redox activity and easy availability. Moreover, the electrochemical properties of PPy can further be enhanced by compositing with CNTs, graphene or their hybrid/composites. Recently, Yesi *et al.* prepared films of CNT-PPy core–shell composite by growing CNTs directly on carbon cloth (CC) as a skeleton, followed by electropolymerization of PPy on the CNTs [189]. The direct fabrication of CNT-PPy on the flexible CC electrode increased the interfacial conductance and the ion transport between the electrode and electrolyte. The PPy/CNT-CC electrode thus prepared exhibited 1038-F/g gravimetric capacitance per active mass of PPy and up to 486.1 F/g per active mass of the PPy/CNT composite, with excellent mechanical flexibility and cycle stability up to 10 000 cycles with 18% capacitance reduction. At the same time, the corresponding asymmetric supercapacitor (PPy-CNT-CC/CNT-CC) showed a maximum power density of 10 962 W/kg and energy density of 3.9 Wh/kg at 1.4-V potential.

For most solid-state supercapacitors based on freestanding graphene materials, the specific capacitance ranges from 80 to 135 F/g, while the corresponding theoretical value should be around 550 F/g. The observed difference is most probably due to the restacking of graphene sheets, and hence reduced active surface area of the graphene-based electrodes [187]. To overcome the π–π restacking of graphene sheets, numerous attempts have been made to control the electrode structure into, for example, porous 3D graphene hydrogels on Ni foam by CVD or freeze-drying GO. Mitchell *et al.* have further proposed a strategy to produce hierarchical and flexible nanosheets of $NiCo_2O_4$-graphene-oxide composite on nickel foam by using electrochemical deposition [190], which exhibited a specific capacitance of 1078 F/g in 3 M KOH electrolyte at 1-mA discharge current and a relatively poor cyclic stability (almost 45% reduction over 500 cycles). In another attempt to reduce the restacking of graphene layers in a 3D graphene electrode, Li *et al.* fabricated a solid-state asymmetric supercapacitor (ASC) based on flexible electrodes [191]. In this

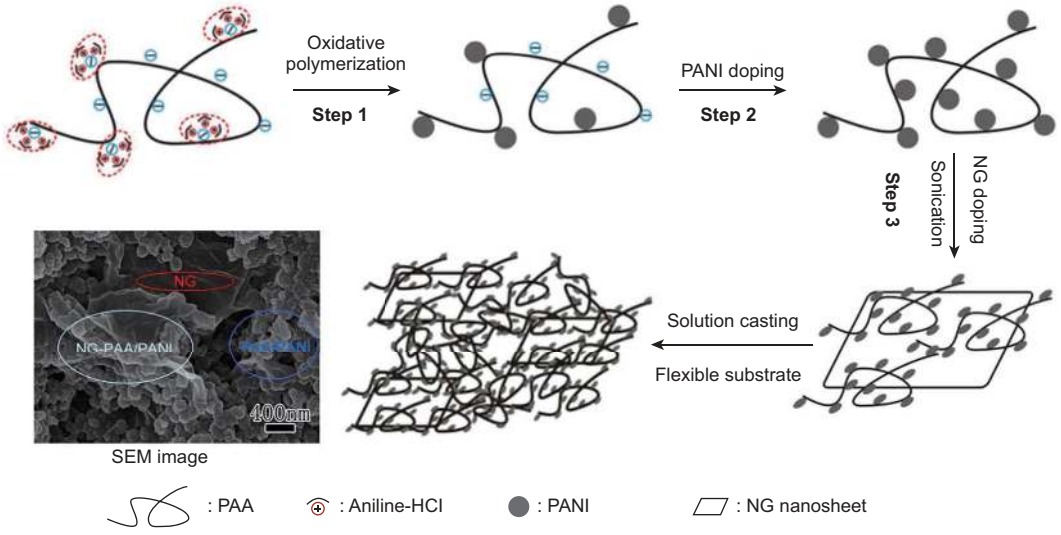

Figure 7. Illustration of the process from synthesis to obtaining a NG-PAA/PANI composite coating on CC; PANI is supplied by both the first and second steps. NG doping in step 3 improves the conductivity further and reduces swelling. Reproduced with permission from ref. [192]. Copyright of Macmillan Publishers Ltd (2016).

case, the positive electrode was made from densely packed graphene sheets with intercalated $Ni(OH)_2$ nanoplates to give a gravimetric capacitance of 573 F/g and volumetric capacitance of 655 F/cm^3 in 1 M KOH electrolyte at 0.2 A/g current density, excellent rate capability and cycling stability. On the other hand, the negative electrode was fabricated with CNT layers stacked in between highly dense graphene sheets. The asymmetric supercapacitor exhibited an energy density of 18 Wh/kg and power density of 850 W/kg at 1-A/g current density. When the current density increased up to 20 A/g, the corresponding energy density remained at 6.4 Wh/kg with a high power density of 17 kW/kg. Bending the device up to 180° caused no influence on the electrochemical performance [191]. With the aim to improve the specific capacitance in film-based FSCs, complex and hybrid structures like CNT/graphene and Mn_3O_4 nanoparticles/graphene paper electrodes with a polymer gel electrolyte of potassium polyacrylate (PAAK)/KCl were conceived and specific capacitance of 72.6 F/g at 0.5 A/g current was obtained [132].

As is the case for conventional ESCs discussed above, composites of CNT/graphene and conducting polymers have also been widely used in FSCs. In particular, Wang *et al.* recently synthesized polyacrylic acid/PANI composites enhanced by nitrogen-doped graphene (NG) (NG-PAA/PANI) [192] and demonstrated that the CC electrodes containing 32 wt.% PANI and 1.3 wt.% NG showed a high capacitance of 521 F/g in 1 M H_2SO_4 electrolyte at 0.5 A/g (Fig. 7). A symmetric supercapacitor fabricated from 20 wt.% PANI-CC electrodes exhibited four times higher capacitance of 68 F/g at 1 A/g than the previously-reported SCs based on flexible PANI-CNT composites. The NG-PAA/PANI electrode retained the full capacitance over large bending angles with an energy density of 5.8 Wh/kg, a power density of 1.1 kW/kg, a superior rate capability of 81% at 10 A/g and long-term electrochemical stability (83.2% retention after 2000 cycles) [192]. By incorporating graphene and CNTs with PPy, Aphale *et al.* fabricated freestanding hybrid electrodes to show a specific capacitance of 453 F/g in 1 M H_2SO_4 at 5 mV/s scan rate (Fig. 8) [193]. Furthermore, the hybrid electrode demonstrated an ultrahigh energy density of 62.96 Wh/kg at a power density of 566.66 W/kg. Four such SCs assembled in a series successfully lit up a 2.2 V LED.

For the fiber-based FSCs, a wearable, fiber-shaped and all-solid-state asymmetric FSC was recently fabricated with a 1.5-V operating voltage using ultrathin MnO_2 nanosheets on carbon fibers as the positive electrode and graphene on carbon fibers as the negative electrode [194], leading to an energy density of 27.2 Wh/kg and power density of 979.7 W/kg. These values are higher than the latest reported for MnO_2-based asymmetric or symmetric supercapacitors, including MnO_2 nanotubes/activated graphene (22.5 Wh/kg at 146.2 W/kg) [195], MnO_2 nanoflowers/Bi_2O_3 nanoflowers (11.3 Wh/kg at 352.6 W/kg) [196], graphene foam (GF)-CNT-MnO_2/GF-CNT-PPy (22.8 Wh/kg at 860 W/kg) [197], 3D

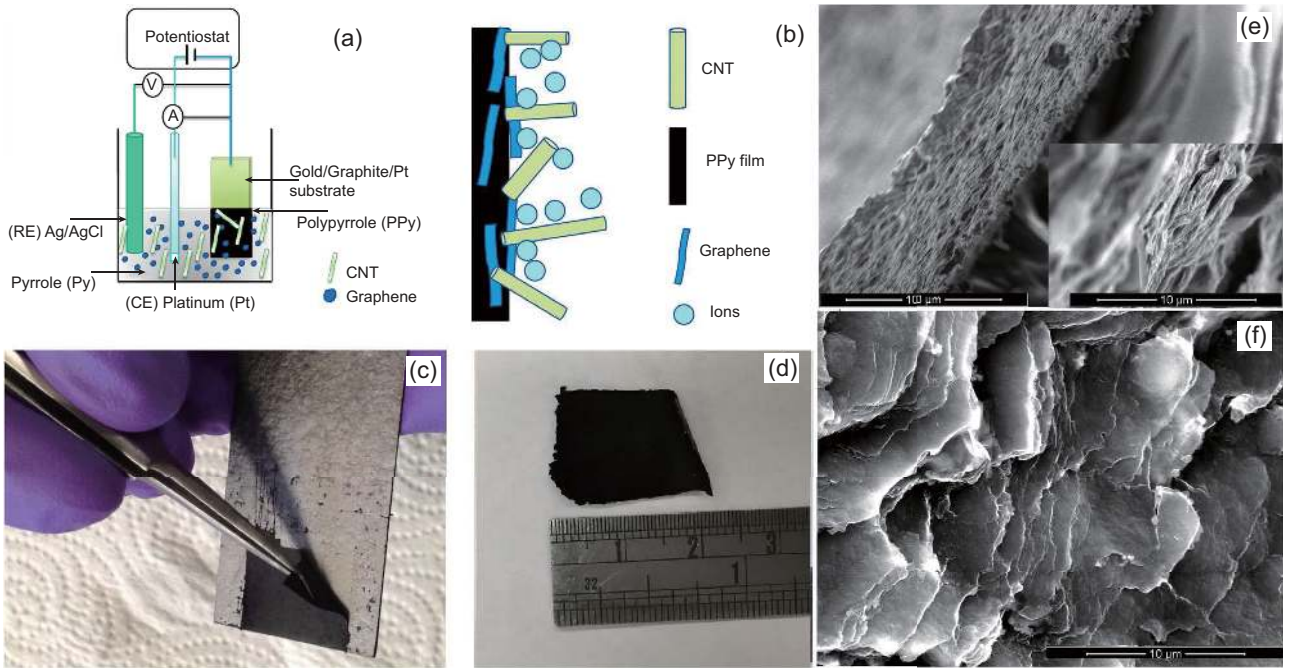

Figure 8. Fabrication and characterization of hybrid electrode. (a) Schematic representing the fabrication process of the nanocomposite electrodes. (b) Illustration of hybrid nanocomposite film forming a unique interface where graphene and CNT are embedded *in situ* during polymerization of PPy. (c, d) Optical image of the actual freestanding film on the graphite substrate with ~2 cm × 2 cm area. (e) Cross-sectional SEM micrograph showing layered formation of the polypyrrole film. (f) Layers of graphene-CNT coated with PPy during polymerization forming a nanocomposite PCG film. Reproduced with permission from ref. [193]. Copyright of Macmillan Publishers Ltd (2016).

graphene-MnO_2/3D graphene-MnO_2 (6.8 Wh/Kg at 62 W/Kg) [198], multilayer MnO_2-GO/porous carbon (energy density of 46.7 Wh/kg at power density of 100 W/kg) [199], 3D MnO_2/graphene hydrogel (21.2 Wh/kg at 0.82 kW/kg) [200] and 2D planar MnO_2/graphene (17 Wh/kg at 2.52 kW/kg) [201]. Moreover, this fiber-shaped asymmetric FSC further displayed sufficiently good bendability and mechanical stability for being connected in parallel and woven into cotton textiles (Fig. 9). By integrating this asymmetric FSC with a nanowire-based photodetector into a self-powered nanodevice, the fiber-shaped asymmetric FSC could efficiently power a photo detector without any requirement for an external bias [194].

Using a silica capillary column as a hydrothermal micro-reactor as depicted in Fig. 10 [202], Yu and coworkers demonstrated a large-scale manufacturing method for continuously producing carbon microfibers with a unique hierarchical structure composed of an interconnected network of CNTs with interposed nitrogen-doped reduced graphene-oxide sheets. The resultant carbon fiber electrode showed an electrical conductivity of 102 S/cm, volumetric capacity of 305 F/cm^3 in sulfuric acid (measured at 73.5 mA/cm^3 in a three-electrode cell) and 300 F/cm^3 in polyvinyl alcohol (PVA)/H_3PO_4 electrolyte (measured at 26.7 mA/cm^3 in a two-electrode cell). The full micro-supercapacitor with PVA/H_3PO_4 gel electrolyte, free from binder, current collector and separator, has a volumetric energy density of 6.3 mWh/cm^3, which is comparable to that of 4 V–500 mAh thin-film lithium battery while maintaining a power density more than two orders of magnitude higher than that of batteries as well as a long cycle life. This fiber-based, all-solid-state micro-supercapacitor was further successfully interfaced into miniaturized flexible devices to power a TiO_2-based ultraviolet photodetector and a light-emitting diode (Fig. 10). Another type of cable/wire-shaped flexible SC, as presented in Fig. 11, was fabricated on a stainless-steel wire using hydrothermal rGO nanosheets [203]. In redox additive electrolyte (PVA/H_3PO_4/Na_2MoO_4), this flexible SC exhibited a maximum length capacitance and energy density of 18.75 mF/cm (areal capacitance of 38.2 mF/cm^2) and 2.6 mWh/cm (areal energy density of 5.3 mWh/cm^2), respectively. The flexibility and stability of the above FSC device have also been investigated and three serially connected devices could be used to light up the green and blue LEDs (Fig. 11) [203]. A similar attempt has been made to demonstrate an rGO-based wearable SC on Cu wire [204]. While recent progress in FSCs is summarized above, interested readers are referred to some earlier review articles on flexible SCs related

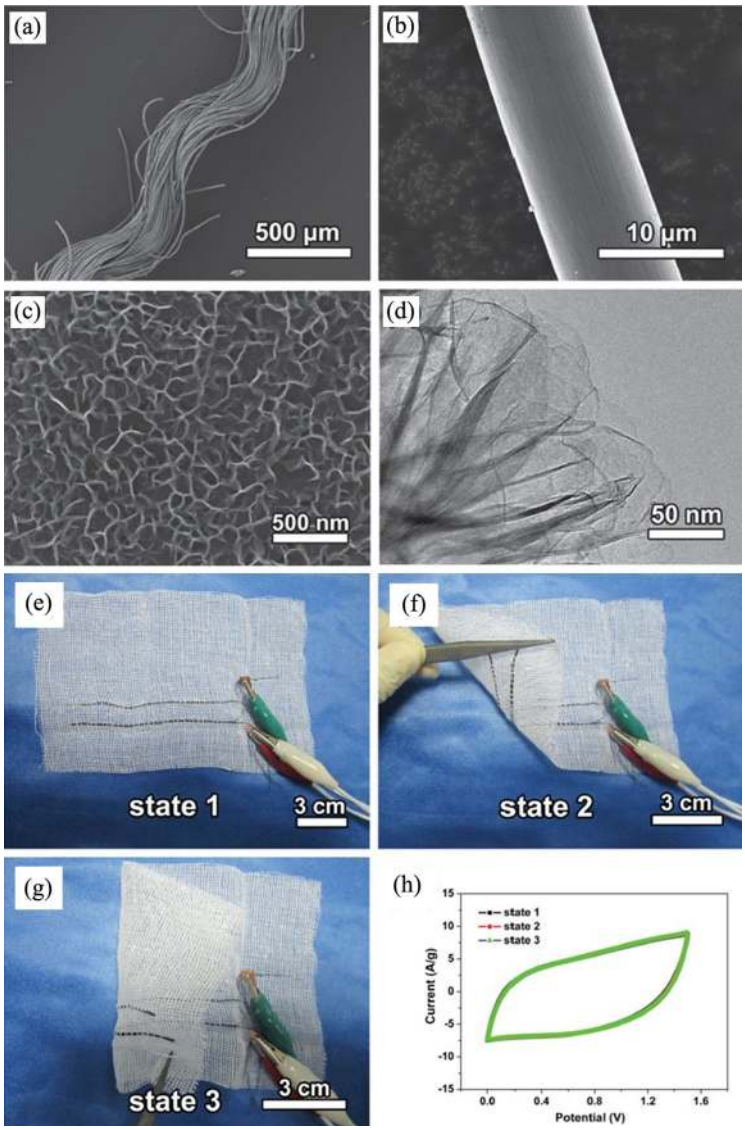

Figure 9. (a) SEM image of carbon fibers bundles. (b, c) SEM image of MnO_2 nanosheet arrays on single carbon fiber at a low and high resolution. (d) TEM of MnO_2 nanosheets. (e–g) Photos of two fiber-shaped ASCs connected in parallel under different bending state which woven into a cotton textile. (h) CV curves of two asymmetric fiber supercapacitors in flat and the corresponding bending states with a scan rate of 100 mV/s. Reproduced with permission from ref. [194]. Copyright of Wiley (2016).

to MnO_2 [205] and carbon materials [188,196], respectively.

Carbon-based stretchable and twistable supercapacitors (film-/fiber-shaped)

Along with the FSCs described above, stretchable and twistable FSCs are needed for advanced electronics, including polymer-based self-powered sensors, polymer light-emitting diodes, polymer solar cells and active matrix displays, to name a few [196]. As well as early reports on stretchable SCs, buckled SWNT/polydimethylsiloxane (PDMS) electrodes have drawn considerable attention, as they could show a strain up to 140% without any change in resistance [206,207]. The use of crumpled graphene papers reduced the cost and complexity for fabricating stretchable and high-performance electrodes for SCs [208,209]. The crumpled-graphene-paper-based electrode demonstrated high stretchability up to 300% linear strain and 800% aerial strain with a high specific capacitance of 196 F/g in H_3PO_4-PVA electrolyte and reliability up to 1000 stretch/relax cycles [208].

In addition, Kim *et al.* have reported a delamination-free stretchable supercapacitor, in which all the component layers were prepared with a single matrix composed of an ionic liquid, 1-ethyl-3-methylimidazolium bis(trifluoromethylsulfonyl)-imide, and a polymer, poly(vinylidene fluoride-hexafluoropropylene), as an electrolyte and a supporting layer, respectively, in the stretchable supercapacitor [210]. The electrode layer was fabricated by incorporating CNTs in the common (polymer) matrix with all the layers being seamlessly fused into one body by dissolving the surface of the composite with acetone. The operational cell voltage was as high as 3 V due to the use of ionic liquid-based gel electrolytes. Specific electrode capacitance and areal cell capacitance were 67.2 F/g and 12.7 F/cm^2, respectively. The standard deviations of the capacitance were only ±2.1% and ±1.4%, respectively, after 500 cycles of the lateral and radial stretches at 0.5 strain.

Polypyrrole (PPy)-coated MnO_2 nanoparticles were deposited onto CNT-based textile supercapacitor electrodes, which increases by 38% the electrochemical energy storage of MnO_2/CNT-based flexible (13% bend) and stretchable (21% tensile strain) supercapacitors (Fig. 12) [211]. A specific capacitance of 461 F/g in H_3PO_4-PVA electrolyte was reported at 0.2-A/g current density, which was attributed to the delamination prevention of MnO_2 nanoparticles by PPy coating. Furthermore, the capacitance retention was 96.2% even after 750 000 bending (13%) cycles [211].

A thin SWNT film and a honeycomb PDMS structure have been utilized as electrode materials and stretchable substrate supports for fabricating stretchable micro-supercapacitors (MSC) [212]. An array of 4 × 4 MSCs showed that the maximum strain in the MSC regions was almost 5 orders of magnitude lower than that the applied strain (of about 150%), and the device capacity remained same even at 150% stretch. Yun and coworkers constructed a stretchable MSC of practical significance, where a stretchable patterned graphene gas sensor driven by integrated micro-supercapacitor array on

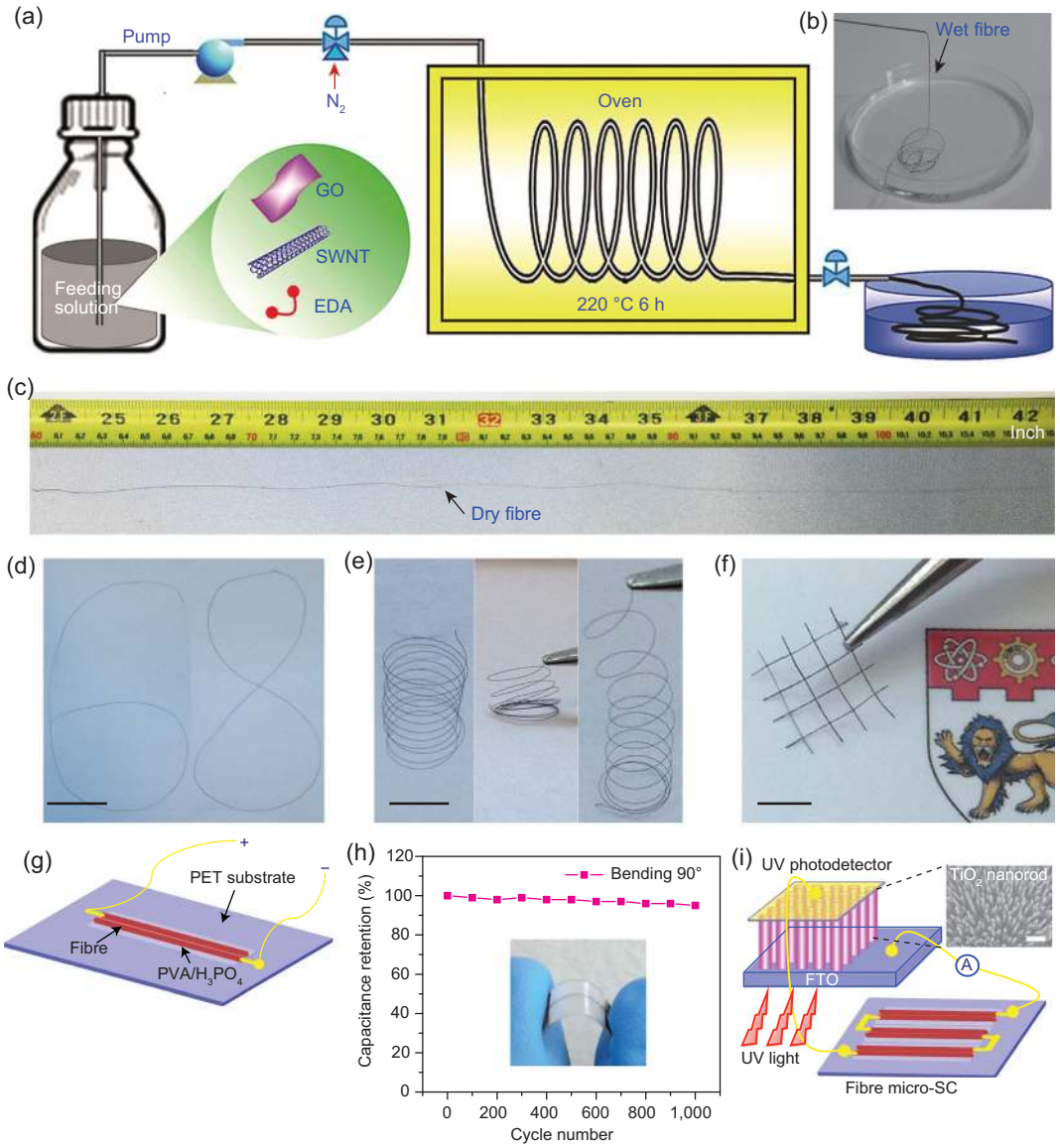

Figure 10. (a) Schematic of the fiber synthesis process by injecting a homogeneous solution containing acid oxidized SWNTs, GO and EDA through a pump into a flexible silica capillary column, followed by in-situ thermal treatment in an oven at 220°C for 6 h before a continuous fiber was pushed into a water reservoir by a pressurized nitrogen flow. (b) Photograph of the as-prepared fibers collected in water. (c) A dry fiber with diameter of ∼50 mm and length of ∼0.5 m (∼20 inches). (d) Planar structures obtained by bending fibers. (e) Compressed and stretched fiber springs. (f) A knitted textile fabricated from fibers. All scale bars: 0.5 cm. (g) Schematic of a micro-SC constructed using two fiber-3 electrodes on a polyester (PET) substrate. (h) Capacitance retention after 1000 cycles up to 908 bending angle. Inset: Photograph of a bent micro-SC. (i) Current response assembly of the ultraviolet photodetector based on the TiO_2 nanorod array powered by the micro-SC. Reproduced with permission from ref. [202]. Copyright of Macmillan Publishers Ltd (2014).

the same deformable substrate, as demonstrated in Fig. 13 [213]. The patterned MSCs, which consisted of PANI-wrapped multiwalled carbon nanotubes (MWNTs) and an ion-gel electrolyte of poly(ethylene glycol)diacrylate and 1-ethyl-3-methylimidazoliumbis (trifluoro-methylsulfonyl) imide, exhibited excellent electrochemical performance under a uniaxial strain of 50% and a biaxial strain of 40%; their initial performance (capacitance of 6.1 F/cm^3 at 5-mA/cm^3 current) characteristics were retained even after1000 cycles of repetitive uniaxial (50%) and biaxial (40%) stretching. Moreover, the patterned graphene sensor successfully detected NO_2 gas for longer than 50 min via integration with MSCs using the serpentine interconnections even under uniaxial stretching by 50%. Such a hybrid combination of SCs with other practical electronic devices is highly desirable for near-term

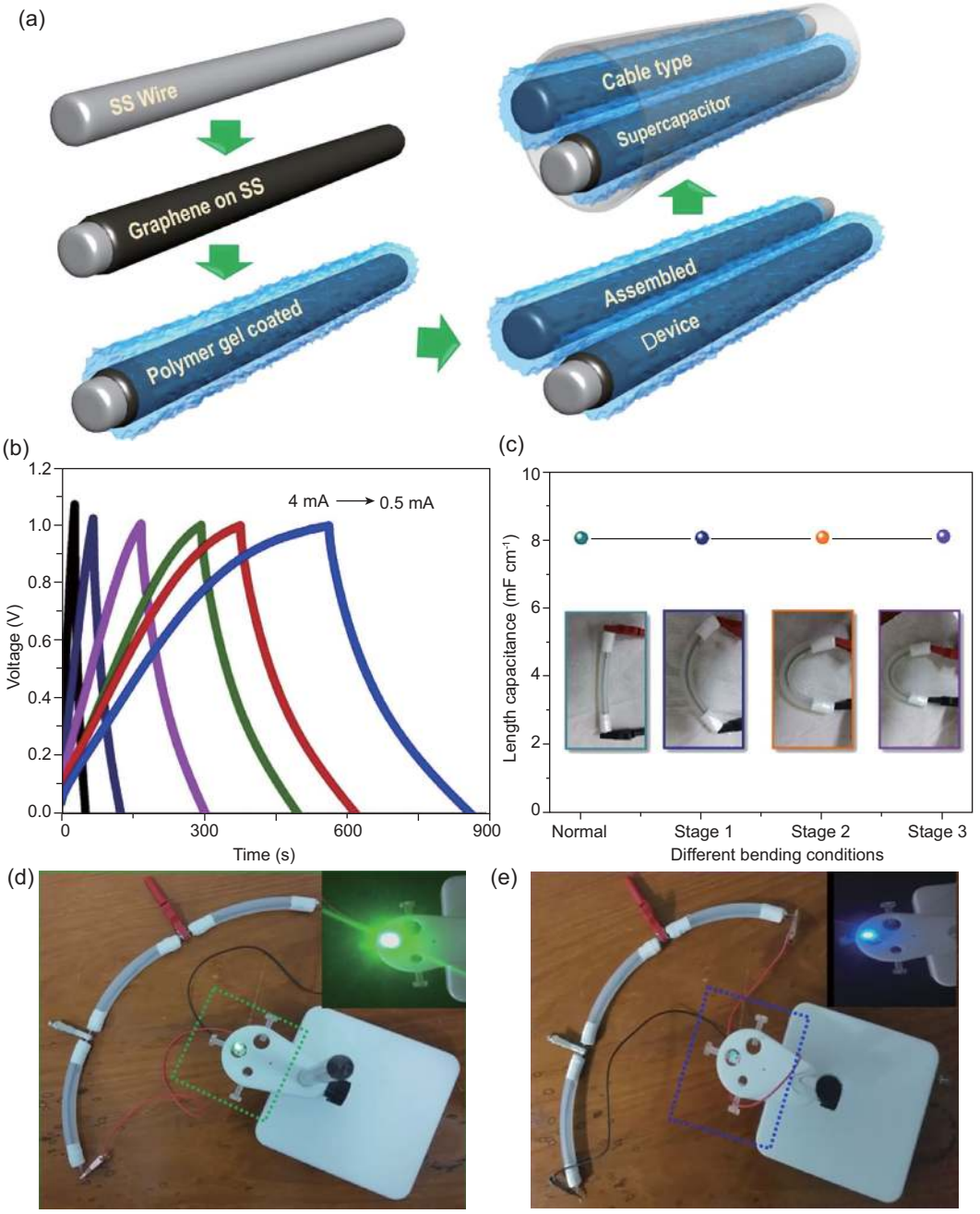

Figure 11. (a) Schematic illustration of fabrication of rGO-based cable supercapacitor using PVA/H_3PO_4/Na_2MoO_4 electrolyte. (b) Galvanostatic charge–discharge curves at the different current densities (0.5–4 mA) for the fabricated cable SC. (c) Capacitance variation at the different bending states. Inset of (c): digital images of the different bending states. (d, e) Demonstration of three serially connected devices can power the green and blue LEDs, respectively. Reproduced with permission from ref. [203]. Copyright of Elsevier (2016).

applications. However, much more attention must be given to further improving capacitive storage capability in flexible and stretchable supercapacitors.

Buckled CNT film was also investigated for stretchable electrodes in SCs, as shown in Fig. 14a–c [214]. A comparative study between PANI composites of buckled CNT with and without nitric acid treatment revealed that acid-treated buckled CNT@PANI electrodes exhibited a higher specific capacitance of 1147.12 mF/cm^2 in H_3PO_4-PVA electrolyte at 10 mV/s [214]. This observation can be correlated with the formation of better interfacial bonding between acid-treated CNTs and PANI. The acid-treated electrode also showed an energy

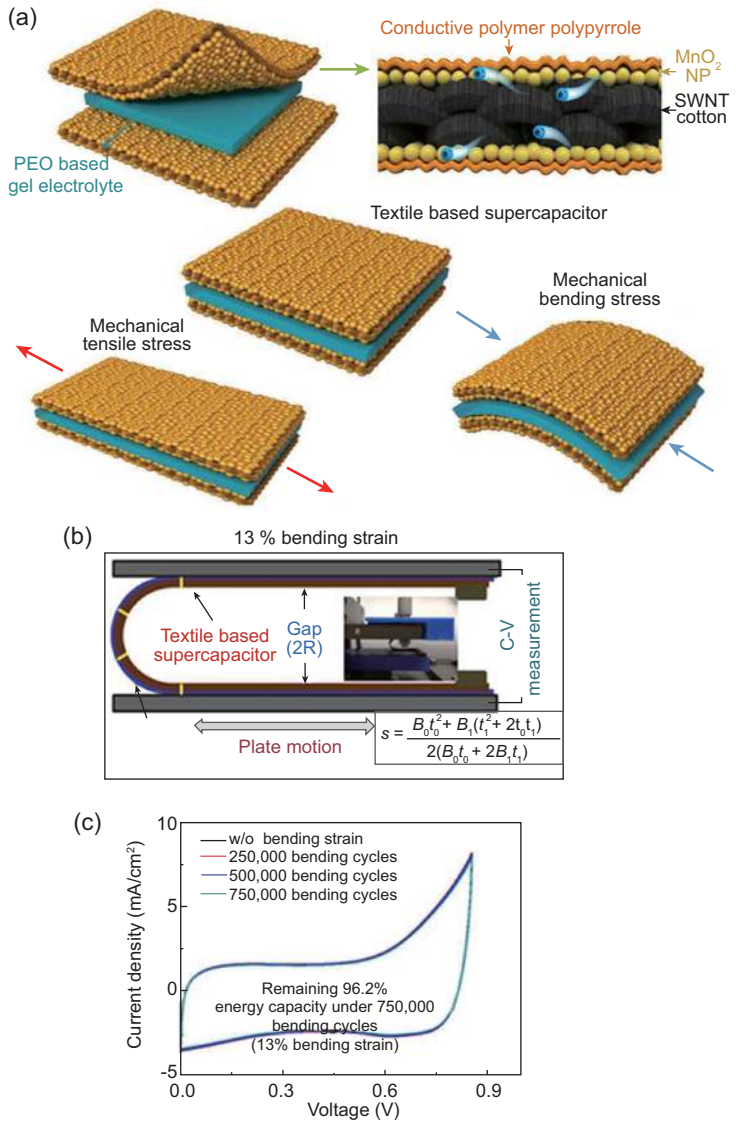

Figure 12. (a) Schematic illustration of the fabrication of polpyrrole—MnO_2-coated textile supercapacitor. (b) Schematic for bending test was performed on polypyrrole—MnO_2-coated supercapacitor. (c) Cyclic voltammetry of supercapacitor under 13% bending strain. Reproduced with permission from ref. [211]. Copyright of American Chemical Society (2015).

density from 31.56 to 50.98 μWh/cm^2 with power density changing from 2.294 to 28.404 mW/cm^2 at the scan rate of 10–200 mV/s. The corresponding supercapacitor sustained an omnidirectional strain of 200%.

In the case of fiber-shaped stretchable and twistable SCs, recently, yarn-based SCs have been demonstrated, which consist of core–shell-structured coiled electrodes with pseudocapacitive CNT-cores and MnO_2-shells, as shown in Fig. 14d and e [215]. The linear and volumetric capacitances of the coiled yarn were determined to be 2.72 mF/cm and 34.6 F/cm^3, respectively. Interestingly, around 84% of its static capacitance was retained after being reversibly stretched by 37.5% strain, while 96.3% dynamic capacitance was maintained during 20% strain deformation despite the extremely high strain rate of 6%/s. The yarn supercapacitors exhibited 95% or 98.8% capacitance retentions after many stretching/releasing or charge/discharge cycles [215]. Stretchable coaxial fiber-shaped SCs have also been fabricated using CNT sheets wrapped on an elastic fiber using a polymer gel sandwiched between the two coaxial CNT layers as the electrolyte and separator as well [216,217].

Transparent SCs have also become important for various optoelectronic applications. Indeed, transparent energy-storage devices are highly desirable for automobile/building windows or personal electronics with high aesthetic appeal. In this regard, a simple dry press transfer technique has been used to transfer thin SWNT films to transparent substrates to prepare transparent and flexible EDLCs with a transparency of 92% at 550 nm and high transparency over visible light and near infrared (NIR) wavelengths [218]. The resultant films showed an extremely high mass specific capacitance of 178 F/g (which is 482 F/g when calculated per mass of carbon) in PVA/H_3PO_4 electrolyte and area specific capacitance of 552 μF/cm^2 compared to other reported carbon-based flexible and transparent EDLCs [219]. The films were also highly stable in terms of specific capacitance over 10 000 loading cycles [218]. Chen *et al.* also fabricated graphene-based transparent and flexible SCs [209], which are attractive for various portable electronic devices. Table 3 summarizes carbon-based flexible, stretchable, wearable as well as transparent supercapacitors.

The advantages of using carbon materials for supercapacitor electrodes lay in the facts that they are highly conductive, binder-free and flexible with a large surface area and excellent properties intrinsically associated with different carbon allotropes. Carbon materials are Earth-abundant and environmentally friendly with respect to metal- or polymer-based electrode materials. Through using flexible carbon materials in supercapacitors, it would be possible to reduce the unnecessary use of metal foils (such as Al) as the current collector. It is also possible to eliminate polymer-binders or other conductive additives. Therefore, the use of carbon materials can propel the flexible supercapacitors to be lighter, portable and more easily manufactured. For many practical applications, however, their efficiencies still need to be improved by combining flexible carbon materials with pseudocapacitive materials (such as, metal oxides and polymers).

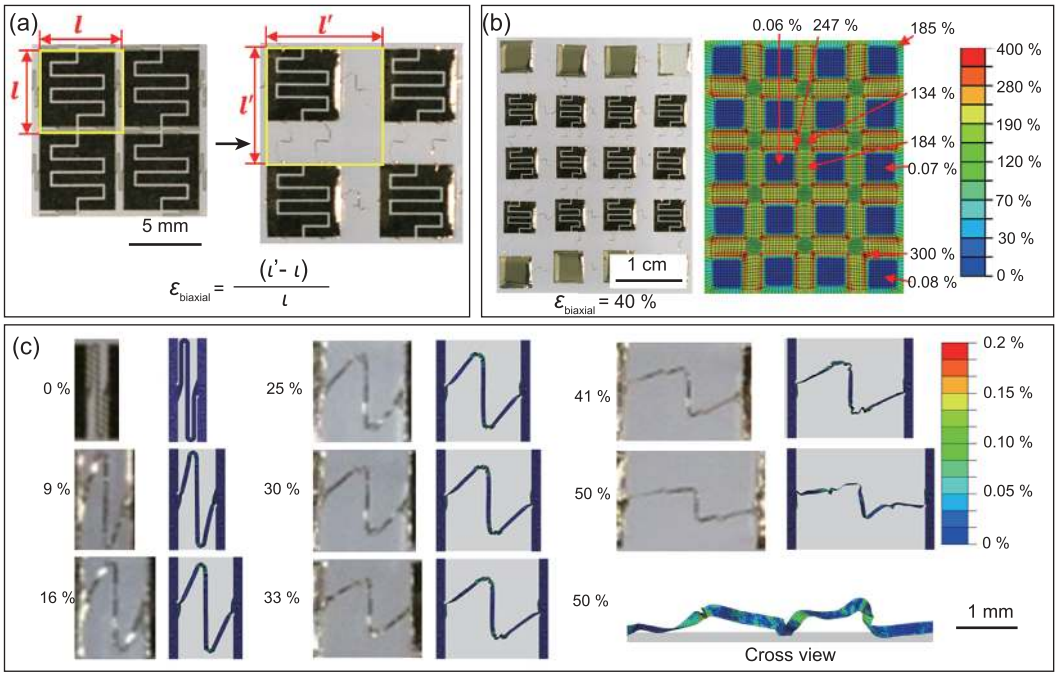

Figure 13. (a) Schematic definition of the biaxial strain $\varepsilon_{biaxial}$. (b) Optical microscope image of the MSC array (left) and the strain distribution estimated by FEM analysis (right) under a biaxial strain of 40%. (c) Optical images (left) and the results obtained from FEM analysis (right) of a serpentine interconnection in various uniaxial stretching states. The cross-sectional view shown is for a strain of 50%. Reproduced with permission from ref. [213]. Copyright of Elsevier (2016).

Carbon-based ultrafast supercapacitors for ac-line filtering

Alternating current (ac)-line filtering by using ultrafast supercapacitors is essential for domestic power usage in order to remove undesired high-frequency noises. ac electricity has a frequency of either 50 or 60 Hz. The combination of various nonlinear loads from different electronic devices in domestic requirements, portable electronics, automobiles and medical appliances often induces higher-order harmonics (>120 Hz) of the basic generating frequency [220]. In order to protect electronic devices from such voltage ripples, aluminum electrolyte capacitors (AECs) are used for ac-line filtering [221–223]. However, AECs have low specific capacitance, and hence occupy a large space and volume in electronic circuits. In this regard, supercapacitors, possessing specific capacitance of 2–5 orders higher in magnitude than that of AECs, could be used for effective ac-line filtering with very negligible occupied space or volume in capacitive components [224,225]. A supercapacitor generally acts like a resistor at 120 Hz after being introduced into transmission lines [223]. The typical resistor–capacitor (RC) time constant for a supercapacitor is around 1 s, associated with the high electrochemical series resistance and microporous structure of supercapacitor electrodes, which is far too long to be useful for the common application of 120-Hz filtering (∼ 8.3 ms period)—indicating the necessity for smoothing the leftover ac ripples in most line-powered electronics [226]. This is mainly because of the fact that unsuitable pore structures of supercapacitor electrodes impede high-rate ion diffusions or their high resistances restrict efficient charge transfer [227]. Thus, the design and fabrication of highly conductive electrodes with optimized micro-/nano-architectures for facile electron/ion transportations can improve the performance for ac-line filtering. Thus, high-surface-area materials with less inherent porosity have been studied for such applications.

Among a variety of other electrode materials, including onion-like carbon [228] and CNTs [229,230], carbide-derived carbon [231], metal oxides [232], polymers [233] and mesoporous carbons [225], utilized to improve related rate capability for ac-line filtering, graphene-based materials and graphene/CNT hybrid structures have recently emerged to be promising over conventional carbon materials because of their superior electrical conductivity and high specific surface area [227,234,235]. Graphene and porous carbon composites have also been demonstrated to be excellent ac-line filters, though their energy-storage capabilities still need to be improved [236].

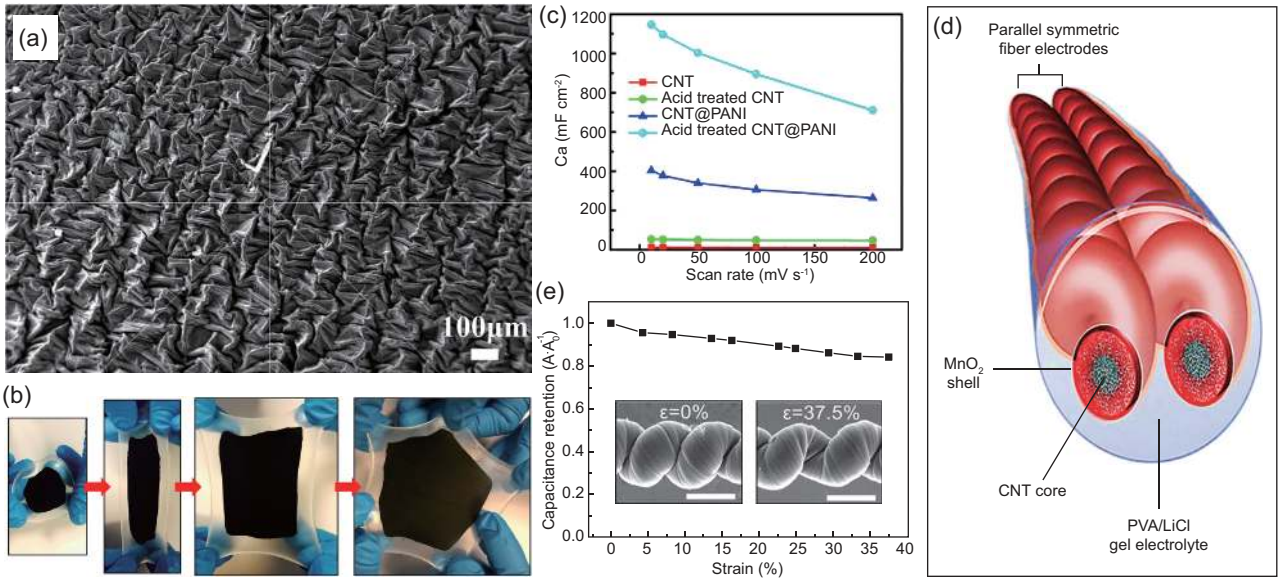

Figure 14. (a) SEM images of buckled structures formed in CNT films at 50% omnidirectional prestrain. (b) Digital images of buckled CNT film at various stretching states. (c) Specific capacitance variation for CNT/PANI SCs with scan rate. Reproduced with permission from ref. [214]. Copyright of American Chemical Society (2016). (d) Schematic illustration for the complete solid-state coiled supercapacitor, which comprises two symmetric MnO_2/CNT core-shell-coiled electrodes and gel electrolyte. (e) Stress loading/unloading curves of the hybrid MnO_2/CNT coiled electrode with tensile strains from 20% to 40%. Reproduced with permission from ref. [215]. Copyright of Wiley (2016).

Lim *et al.* recently demonstrated that the substitutional pyridinic nitrogen dopant sites in carbon nanotubes can selectively initiate the unzipping of CNT side walls at a relatively low electrochemical potential (0.6 V) [235]. The resultant nanostructures consisting of partially zipped and/or unzipped graphene nanoribbons wrapping around carbon nanotube cores maintain the intact 2D crystallinity with well-defined atomic configuration at the unzipped edges (Fig. 15). The synergistic interaction between the large surface area and robust electrical connectivity of the unique nanoarchitecture led to ultrahigh-power supercapacitor performance, which can serve for ac filtering with the record high-rate capability of 85° (very close to that of AECs, 83.9°) of phase angle at 120 Hz. Lin *et al.* also fabricated a 3D graphene/CNT carpet (G/CNTC)-based micro-supercapacitor on nickel electrodes [237]. The G/CNTC showed an 81.5° phase angle at a 120-Hz frequency. However, much work still needs to be done in order to realize supercapacitors having both ac-line-filtering capability and excellent charge-storage capability for practical applications.

SUMMARY AND PERSPECTIVES

Carbon nanomaterials, including 1D CNTs, 2D graphene, 3D mesoporous carbon and their composites with conductive polymers or metal oxides, have been widely used as electrodes in supercapacitors, such as EDLCs, PCs and HSCs. Generally speaking, pure carbon nanomaterials without any functional groups are useful as EDLC-electrodes because of their high specific surface area and excellent electrical conductivity. The advantages of EDLC include its high-rate capability and outstanding cyclic stability (e.g. retention of 95%∼100% after 1000∼10 000 cycles). The specific capacitance for pure carbon nanomaterials in EDLC has been demonstrated to be in the range of 10–300 F/g. For carbon-composite nanomaterials, the specific capacitance can be increased by one order of magnitude: generally 100∼1000 F/g. By compositing carbon nanomaterials with other materials having pseudo-capacitances (e.g. conducting polymers, metal oxides or hydroxyls), therefore, the energy density can be largely improved, but their rate capability and cyclic stability may decrease to 60–90% after 1000 cycles.

Numerous recent efforts have been made to improve the electrochemical performance of the supercapacitors based on carbon nanomaterials by improving their specific capacitance, energy density, power density, rate capability and/or cyclic stability. The design and development of advanced 3D electrode structures and compositing carbon nanomaterials with other active materials have been demonstrated to be effective approaches to high-performance carbon-based SCs. Hybrid supercapacitors can fill the gap between a supercapacitor and a

Table 3. Carbon nanomaterials in flexible, stretchable, wearable and transparent supercapacitors.

Electrode	Electrolyte	Specific capacitance	Power density	Energy density	Retention capability	Ref.
(i) Flexible						
CNT-graphene/Mn_3O_4-graphene (flexibility: bendable and twistable)	Potassium polyacrylate (PAAK)/KCl	72.6 F/g at 0.5 A/g current	9 kW/kg	22.9 Wh/kg	86% after 10 000 cycles at 10 mV/s	132
MnO_2/carbon nanofiber	PVA-KOH, PVA-$H_4SiW_{12}O_{40}\cdot nH_2O$	100 F/g, 142 F/g at 5 mV/s scan	–	–	60%, 28% at 100 mV/s	183
TiO_2/MWCNT	1 M H_2SO_4	36.8 F/g at 20 mV/s scan	–	–		184
Porous carbon nanofibers (flexibility: no degradation after 100 times complete bending)	0.5 M H_2SO_4	104.5 F/g at 0.2 A/g current	600 W/kg	3.22 Wh/kg	94% after 2000 cycles at 1 A/g	186
MnO_2 nanotune/CNT (flexibility: no degradation on bend and twist)	Polyvinyl alcohol (PVA)/LiCl	29.3 F/g at 0.5 mA/cm^2 current	13.8 mW/cm^3	0.45 mWh/cm^3	105% after 6000 cycles at 1.2 mA/cm^2	187
CNT (core)/PPy(shell) (flexibility: no degradation after 20 bending cycles)	0.5 M H_2SO_4	486.1 F/g at 1.25 A/g current	10.96 kW/kg	3.9 Wh/kg	82% after 10 000 cycles at 8 A/g	189
$NiCo_2O_4$-GO (flexibility: no degradation up to 180° bending and complete twisting)	3 M KOH	1078 F/g at 1 mA current	–	–	∼58% after 100 cycles at 3 mA	190
$Ni(OH)_2$/dense stack of graphene sheets (flexibility: no degradation up to 180° bending)	1 M KOH	573 F/g at 0.2 A/g current	8.5 kW/kg	9 Wh/kg	89% after 2000 cycles	191
N-doped graphene- polyacrylic acid (PAA)/PANI (flexibility: no degradation up to 135° bending)	1 M H_2SO_4, H_2SO_4-PVA	521 F/g at 0.5 A/g current	1.1 kW/kg	5.8 Wh/kg	83.2% after 2000 cycles at 1 A/g	192
PPy/CNT-graphene (flexibility: not demonstrated)	1 M H_2SO_4	453 F/g at 5 mV/s scan	566.66 W/kg	62.96 Wh/kg	–	193
rGO coated on stainless-steel wire (flexibility: no degradation after 180° bending)	PVA/H_3PO_4/Na_2MoO_4 polymer gel	38.2 mF/cm^2 at 0.5 mA current	5.3 microWh/cm^2	63.7 microW/cm^2	100% after 2500 cycles	203
(ii) Flexible and wearable						
MnO_2 sheets/carbon fiber (flexibility: highly flexible wire without any degradation on bending)	PVA-LiCl	634.5 F/g at 2.5 A/g current	979.7 W/kg	27.2 Wh/kg	95.2% after 3000 cycles at 20 A/g	194
SWNT/N-doped rGO fiber (flexibility: 97% of capacitance retention after 1000 times bending at 90°)	1 M H_2SO_4	305 F/cm^3 at 26.7 mA/cm^3 current	1.085 W/cm^3	6.3 mWh/cm^3	93% after 10 000 cycles at 250 mA cm/^{3}	202
Graphene aerogel on Cu wire (flexibility: 99% of capacitance retention after 1000 times bending at 160°)	Polyvinylpyrrolidone (PVP)	12.5 F/cm at 5 mV/s scan	–	–	95% after 10 000 cycles at 1 A/g	204

Table 3. *Continued.*

Electrode	Electrolyte	Specific capacitance	Power density	Energy density	Retention capability	Ref.
(iii) Flexible/wearable and stretchable						
Buckled SWNT macrofilm (no degradation after 30% strain)	1 M Et_4NBF_4/ propylene carbonate	54 F/g at 1 A/g current	1 kW/kg	∼3.5 Wh/kg	96.3% after 1000 cycles with 30% strain at 1 A/g	206
SWNT/polydimethylsiloxane (PDMS) (can sustain 120% strain)	H_2SO_4-polyvinyl alcohol (PVA)	53 F/g at 10 A/g current with 120% strain	32 kW/kg	–	100% after 1000 cycles under 120% strain	207
Crumpled graphene hydrogel (can sustain 300% linear and 800% areal strain)	H_3PO_4-PVA	166–196 F/g at 1 A/g current	–	30 Wh/kg under 300% axial strain	95% after 1000 stretching cycles with 200% strain	208
Double-walled CNT/poly(vinylidene fluoride-hexafluoropropylene (can sustain 50% lateral strain)	1-ethyl-3-methylimidazolium bis(trifluoromethyl-sulfonyl)imide	67.2 F/g at 2.5 A/g current	3.7 kW/kg	20.3 Wh/kg with 50% lateral strain	97.9% after 500 cycles of 50% lateral strain	210
PPy-MnO_2/CNT textile (can sustain 21% tensile and 13% bending strains)	H_3PO_4-PVA	461 F/g at 0.2 A/g current	22.1 kW/kg	31.1 Wh/kg	96.2% after 750 000 bending (13%) cycles	211
SWNT/honeycomb PDMS (can sustain 150% stretch)	H_3PO_4-PVA	3.3 F/cm^3 at 10 V/s scan	–	–	100% after 150% stretch	212
PANI/MWCNT (can sustain 50% uniaxial strain and 40% biaxial strain)	poly(ethylene glycol)diacrylate/ Et_4NBF_4	6.1 F/cm^3 at 5 mA/cm^3 current	3 mW/cm^3	3.2 mWh/cm^3	Within 95% up to 1000 cycles of 50% uniaxial strain	213
Buckled CNT/PANI (can sustain 200% strain)	H_3PO_4-PVA	364.6 F/g at 10 mV/s scan.	2.34 to 30.04 mW/cm^2	30.2 to 54.6 μWh/cm^2	96.9% after 20 stretching cycles	214
MnO_2-CNT (shell)/nylon (core) (can sustain 150% strain)	PVA-LiCl	5.4 mF/cm (linear), 40.9 mF/cm^2 (areal)	66.9 μW/cm^2	2.6 μWh/cm^2	87.8% with 17.1% strainsfor 0–120% strain cycles	215
CNT sheets coated on elastic fiber (can sustain up to 75% strain)	H_3PO_4-PVA	41.4 F/g at 0.1 A/g current	421 W/kg	0.363 Wh/kg	95% after 100 stretching cycles at 75% strain	216
PEDOT-PSS/CNT/Elastic wires (can sustain up to 350% strain)	H_3PO_4-PVA	122.8 F/g at 0.5 A/g current	–	–	106% after 100 stretching cycles with 200% strain	217
(iv) Flexible/stretchable and transparent						
In_2O_3 nanowire/CNT (∼60% transparent at 600 nm and flexible)	1 $MLiClO_4$	64 F/g at 0.5 A/g	7.48 kW/kg	1.29 Wh/kg	82.8% after 500 cycles at 0.5 A/g	182

Table 3. *Continued.*

Electrode	Electrolyte	Specific capacitance	Power density	Energy density	Retention capability	Ref.
Wrinkled graphene (57% transparent at 550 nm, can sustain bending and 40% strain)	$PVA/H_3PO_4/H_2O$	7.6 F/g at 1 V/s scan	–	–	100% after 100 cycles with bending or 40% strain	209
SWNT (92% transparent at 550 nm and flexible up to 180°)	PVA/H_3PO_4	178 F/g at 0.53 A/g current	–	–	100% up to 10 000 cycles	218

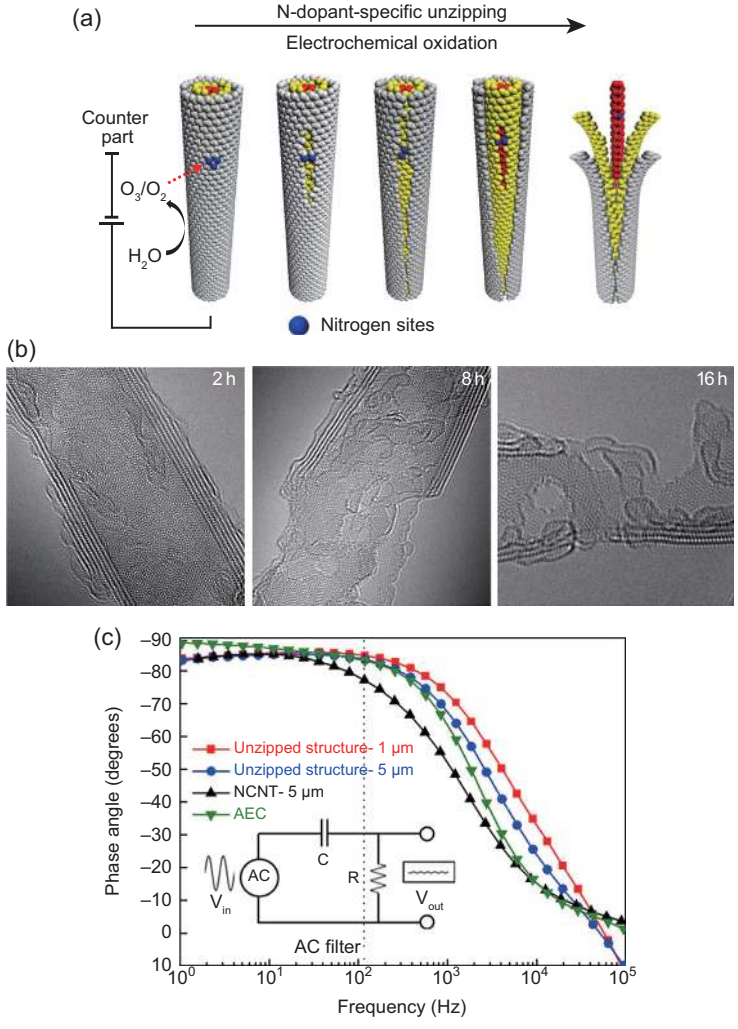

Figure 15. (a) Schematic illustration of N-dopant-specific unzipping of NCNT. (b) Aberration-corrected TEM images of 2, 8 and 16 h unzipped nanostructures (in 1 M H_2SO_4 at 0.8 V) (scale bar: 2 nm). (c) AC impedance phase angle versus frequency; vertical dotted line indicates 120-Hz frequency. Reproduced with permission from ref. [235]. Copyright of Macmillan Publishers Ltd (2016).

battery by improving both energy and power density in a single electrochemical device.

Flexible, stretchable and even transparent supercapacitors are also very important for the next generation of wearable electronics. Although compositing graphene and CNT with appropriate conducting polymers has been demonstrated to be an effective approach towards SCs with excellent flexibility and strain resistance while retaining their electrochemical performance, conducting polymers often lose their inherent electrical properties in composites.

As can be seen from the above discussions, great progress has been achieved in the development of carbon-based supercapacitors, including EDLCs, PCs and HSCs in either traditional or flexible, stretchable and even transparent forms. Compared with batteries, SCs possess a high power density, short charging time, good discharge/charge cyclability and broad-temperature-range applicability. These advantages make SCs useful for various potential applications, including hybrid electric vehicles, renewable-energy-storage gadgets and portable electronics. However, there are still some challenges that need to be addressed to further improve the performance of carbon-based electrodes. First, carbon is well known to have a lower specific capacitance as compared to other pseudocapacitive materials, such as metal oxide and conducting polymers. Therefore, the carbon content, nature of heteroatom dopant(s), if any, and its crystallinity or connectivity of a carbon network within composite electrodes must be well understood in order to obtain high electrode performance. Second, it is also essential to further improve electrolytes and separators for efficient charge storage as well as high-rate capability and cycling stability. Third, SCs with excellent ac-line-filtering capability still need to be developed to bring advanced SC technologies to the marketplace for various practical applications, ranging from self-powered wearable optoelectronics to electrical vehicles. Finally, the energy and power densities of

SCs need to be further improved while their weight, volume and cost to be further reduced.

ACKNOWLEDGEMENTS

We would like to thank colleagues, collaborators and peers for their work cited in this article.

FUNDING

This work is supported by the National Science Foundation (NSF-CMMI-1400274), the Air Force Office of Scientific Research (AFOSR-AF9550–12–1–0069), the Department of Defense—Multidisciplinary University Research Initiative (DoD-MURI-FA9550–12–1–0037) and the Dayton Area Graduate Studies Institute (DAGSI-RQ20-CWRU-13–4).

Conflict of interest statement. None declared.

REFERENCES

1. Dai L, Chang DW and Baek JB *et al.* Carbon nanomaterials for advanced energy conversion and storage. *Small* 2012; **8**: 1130–66.
2. Yang Z, Ren J and Zhang Z *et al.* Recent advancement of nanostructured carbon for energy applications. *Chem Rev* 2015; **115**: 5159–223.
3. Zhu J, Yang D and Yin Z *et al.* Graphene and graphene-based materials for energy storage applications. *Small* 2014; **10**: 3480–98.
4. Cao X, Yin Z and Zhang H. Three-dimensional graphene materials: preparation, structures and application in supercapacitors. *Energy Environ Sci* 2014; **7**: 1850–65.
5. Huang X, Tan C and Yin Z *et al.* 25th anniversary article: hybrid nanostructures based on two-dimensional nanomaterials. *Adv Mater* 2014; **26**: 2185–204.
6. Tan C and Zhang H. Two-dimensional transition metal dichalcogenide nanosheet-based composites. *Chem Soc Rev* 2015; **44**: 2713–31.
7. Huang X, Zeng Z and Zhang H. Metal dichalcogenide nanosheets: preparation, properties and applications. *Chem Soc Rev* 2013; **42**: 1934–46.
8. Miller JR and Simon P. Materials science: electrochemical capacitors for energy management. *Science* 2008; **321**: 651–2.
9. Odom TW, Huang JL and Kim P *et al.* Atomic structure and electronic properties of single-walled carbon nanotubes. *Nature* 1998; **391**: 62–4.
10. Cherusseri J, Sharma R and Kar KK. Helically coiled carbon nanotube electrodes for flexible supercapacitors. *Carbon* 2016; **105**: 113–25.
11. Graham AP, Duesberg GS and Hoenlein W *et al.* How do carbon nanotubes fit into the semiconductor roadmap? *Appl Phys A* 2005; **80**: 1141–51.
12. Yu MF, Files BS and Arepalli S *et al.* Tensile loading of ropes of single wall carbon nanotubes and their mechanical properties. *Phys Rev Lett* 2000; **84**: 5552–5.
13. Demczyk BG, Wang YM and Cumings J *et al.* Direct mechanical measurement of the tensile strength and elastic modulus of multiwalled carbon nanotubes. *Mater Sci Eng A* 2002; **334**: 173–8.
14. Ebbesen T, Lezec H and Hiura H *et al.* Electrical conductivity of individual carbon nanotubes. *Nature* 1996; **382**: 54–6.
15. Yang Z, Chen T and He R *et al.* Aligned carbon nanotube sheets for the electrodes of organic solar cells. *Adv Mater* 2011; **23**: 5436–9.
16. Pop E, Mann D and Wang Q *et al.* Thermal conductance of an individual single-wall carbon nanotube above room temperature. *Nano Lett* 2006; **6**: 96–100.
17. Kim P, Shi L and Majumdar A *et al.* Thermal transport measurements of individual multiwalled nanotubes. *Phys Rev Lett* 2001; **87**: 215502.
18. Chen T, Cai Z and Yang Z *et al.* Nitrogen-doped carbon nanotube composite fiber with a core–sheath structure for novel electrodes. *Adv Mater* 2011; **23**: 4620–5.
19. Yang Z, Li L and Lin H *et al.* Penetrated and aligned carbon nanotubes for counter electrodes of highly efficient dye-sensitized solar cells. *Chem Phys Lett* 2012; **549**: 82–5.
20. Novoselov KS, Geim AK and Morozov SV *et al.* Electric field effect in atomically thin carbon films. *Science* 2004; **306**: 666–9.
21. Geim AK and Novoselov KS. The rise of graphene. *Nat Mater* 2007; **6**: 183–91.
22. Balandin AA. Thermal properties of graphene and nanostructured carbon materials. *Nat Mater* 2011; **10**: 569–81.
23. Park S and Ruoff RS. Chemical methods for the production of graphenes. *Nat Nano* 2009; **4**: 217–24.
24. Candelaria SL, Shao Y and Zhou W *et al.* Nanostructured carbon for energy storage and conversion. *Nano Energy* 2012; **1**: 195–220.
25. Zhai Y, Dou Y and Zhao D *et al.* Carbon materials for chemical capacitive energy storage. *Adv Mater* 2011; **23**: 4828–50.
26. Dai L. Functionalization of graphene for efficient energy conversion and storage. *ACC Chem Res* 2013; **15**: 31–42.
27. Lee C, Wei X and Kysar JW *et al.* Measurement of the elastic properties and intrinsic strength of monolayer graphene. *Science* 2008; **321**: 385–8.
28. Bolotin KI, Sikes K and Jiang Z *et al.* Ultrahigh electron mobility in suspended graphene. *Solid State Commun* 2008; **146**: 351–5.
29. Stoller MD, Park S and Zhu Y *et al.* Graphene-based ultracapacitors. *Nano Lett* 2008; **8**: 3498–502.
30. Huang X, Qi X and Boeyab F *et al.* Graphene-based composites. *Chem Soc Rev* 2012; **41**: 666–86.
31. Huang X, Yin Z and Wu S *et al.* Graphene-based materials: synthesis, characterization, properties, and applications. *Small* 2011; **7**: 1876–902.
32. Wang G, Liang R and Liu L *et al.* Improving the specific capacitance of carbon nanotubes-based supercapacitors by combining introducing functional groups on carbon nanotubes with using redox-active electrolyte. *Electrochim Acta* 2014: **115**: 183–8.

33. Bai X, Hu X and Zhou S *et al.* In situ polymerization and characterization of grafted poly (3,4-ethylenedioxythiophene)/multiwalled carbon nanotubes composite with high electrochemical performances. *Electrochim Acta* 2013; **87**: 394–400.
34. Yang M, Cheng B and Song H *et al.* Preparation and electrochemical performance of polyaniline-based carbon nanotubes as electrode material for supercapacitor. *Electrochim Acta* 2010: **55**: 7021–7.
35. Hahn M, Baertschi M and Barbieri O *et al.* Interfacial capacitance and electronic conductance of activated carbon double-layer electrodes. *Electrochem Solid-St Lett* 2004; **7**: A33–6.
36. An KH, Jeon KK and Kim WS *et al.* Characterization of supercapacitors using singlewalled carbon nanotube electrodes. *J Korean Phys Soc* 2001; **39**: S511–7.
37. Pan H, Poh CK and Feng YP *et al.* Supercapacitor electrodes from tubes-in-tube carbon nanostructures. *Chem Mater* 2007; **19**: 6120–5.
38. Izadi-Najafabadi A, Yasuda S and Kobashi K *et al.* Extracting the full potential of single-walled carbon nanotubes as durable supercapacitor electrodes operable at 4 V with high power and energy density. *Adv Mater* 2010; **22**: E235–41.
39. Frackowiak E, Metenier K and Bertagna V *et al.* Supercapacitor electrodes from multiwalled carbon nanotubes. *Appl Phys Lett* 2000; **77**: 2421–3.
40. Xiang LL, Jing T and Xin G *et al.* Preparation and supercapacitor performance of nitrogen-doped carbon nanotubes from polyaniline modification. *Acta Phys Chim Sin* 2013; **29**: 111–6.
41. Gueon D and Moon JH. Nitrogen-doped carbon nanotube spherical particles for supercapacitor applications: emulsion-assisted compact packing and capacitance enhancement. *ACS Appl Mater Interfaces* 2015; **7**: 20083–9.
42. Bulusheva LG, Fedorovskaya EO and Kurenya AG *et al.* Supercapacitor performance of nitrogen-doped carbon nanotube arrays. *Phys Status Solidi (B)* 2013; **250**: 2586–91.
43. Chen Y, Zhang X and Zhang D *et al.* High performance supercapacitors based on reduced graphene oxide in aqueous and ionic liquid electrolytes. *Carbon* 2011; **49**: 573–80.
44. Zhang L and Shi G. Preparation of highly conductive graphene hydrogels for fabricating supercapacitors with high rate capability. *J Phys Chem C* 2011; **115**: 17206–12.
45. Jin Y, Huang S and Zhang M *et al.* A green and efficient method to produce graphene for electrochemical capacitors from graphene oxide using sodium carbonate as a reducing agent. *Appl Surf Sci* 2013; **268**: 541–6.
46. Du X, Guo P and Song H *et al.* Graphene nanosheets as electrode material for electric double-layer capacitors. *Electrochim Acta* 2010; **55**: 4812–9.
47. Lv W, Tang DM and He YB *et al.* Low-temperature exfoliated graphenes: vacuum-promoted exfoliation and electrochemical energy storage. *ACS Nano* 2009; **3**: 3730–6.
48. Zhu Y, Murali S and Stoller MD *et al.* Microwave assisted exfoliation and reduction of graphite oxide for ultracapacitors. *Carbon* 2010; **48**: 2118–22.
49. Xu Y, Lin Z and Zhong X *et al.* Holey graphene frameworks for highly efficient capacitive energy storage. *Nat Commun* 2014; **5**: 4554.
50. Zhu Y, Murali S and Stoller MD *et al.* Carbon-based supercapacitors produced by activation of graphene. *Science* 2011; **332**: 1537–41.
51. Zhang LL, Zhao X and Stoller MD *et al.* Highly conductive and porous activated reduced graphene oxide films for high-power supercapacitors. *Nano Lett* 2012; **12**: 1806–12.
52. Kim T, Jung G and Yoo S *et al.* Activated graphene-based carbons as supercapacitor electrodes with macro- and mesopores. *ACS Nano* 2013; **7**: 6899–905.
53. Liu Y, Shen Y and Sun L *et al.* Elemental superdoping of graphene and carbon nanotubes. *Nat Commun* 2016; **7**: 10921.
54. Jeong HM, Lee JW and Shin WH *et al.* Nitrogen-doped graphene for high-performance ultracapacitors and the importance of nitrogen-doped sites at basal planes. *Nano Lett* 2011; **11**: 2472–7.
55. Zhao Y, Hu C and Hu Y *et al.* A versatile, ultralight, nitrogen-doped graphene framework. *Angew Chem Int Ed* 2012; **51**: 11371–5.
56. Han J, Zhang LL and Lee S *et al.* Generation of B-doped graphene nanoplatelets using a solution process and their supercapacitor applications. *ACS Nano* 2012; **7**: 19–26.
57. Wang C, Zhou Y and Sun L *et al.* N/P-codoped thermally reduced graphene for high-performance supercapacitor applications. *J Phys Chem C* 2013; **117**: 14912–9.
58. Ke Q and Wang J. Graphene-based materials for supercapacitor electrodes: a review. *J Materiomics* 2016; **2**: 37–54.
59. Ma Y and Chen Y. Three-dimensional graphene networks: synthesis, properties and applications. *Nat Sci Rev* 2015; **2**: 40–53.
60. Zhao Z, Wang Z and Qiu J *et al.* Three dimensional graphene-based hydrogel/aerogel materials. *Rev Adv Mater Sci* 2014; **36**: 137–51.
61. Xu Y, Sheng K and Li C *et al.* Self-assembled graphene hydrogel via a one-step hydrothermal process. *ACS Nano* 2010; **4**: 4324–30.
62. Chen P, Yang JJ and Li SS *et al.* Hydrothermal synthesis of macroscopic nitrogen-doped graphene hydrogels for ultrafast supercapacitor. *Nano Energy* 2013; **2**: 249–56.
63. Zhang LB, Chen GY and Hedhili MN *et al.* Three-dimensional assemblies of graphene prepared by a novel chemical reduction-induced self-assembly method. *Nanoscale* 2012; **4**: 7038–45.
64. Jiang X, Ma YW and Li JJ *et al.* Self-assembly of reduced graphene oxide into three-dimensional architecture by divalent ion linkage. *J Phys Chem C* 2010; **114**: 22462–5.
65. Xu YX, Wu QO and Sun YQ *et al.* Three-dimensional self-assembly of graphene oxide and DNA into multifunctional hydrogels. *ACS Nano* 2010; **4**: 7358–62.
66. Sun ST and Wu PY. A one-step strategy for thermal- and pH-responsive graphene oxide interpenetrating polymer hydrogel networks. *J Mater Chem* 2011; **21**: 4095–7.
67. Worsley MA, Pauzauskie PJ and Olson TY *et al.* Synthesis of graphene aerogel with high electrical conductivity. *J Am Chem Soc* 2010; **132**: 14067–9.
68. Xie X, Zhou YL and Bi HC *et al.* Large-range control of the microstructures and properties of three-dimensional porous graphene. *Sci Rep* 2013; **3**: 6.
69. Zhu C, Liu T and Qian F *et al.* Supercapacitors based on three-dimensional hierarchical graphene aerogels with periodic macropores. *Nano Lett* 2016; **16**: 3448–56.
70. Jung SM, Mafra DL and Lin CT *et al.* Controlled porous structures of graphene aerogels and their effect on supercapacitor performance. *Nanoscale* 2015; **7**: 4386–93.
71. Hao L, Ning J and Luo B *et al.* Structural evolution of 2D microporous covalent triazine-based framework toward the study of high-performance supercapacitors. *J Am Chem Soc* 2015; **137**: 219–25.
72. Yang X, Cheng C and Wang Y *et al.* Liquid-mediated dense integration of graphene materials for compact capacitive energy storage. *Science* 2013; **341**: 534–7.
73. Yoon Y, Lee K and Kwon S *et al.* Vertical alignments of graphene sheets spatially and densely piled for fast ion diffusion in compact supercapacitors. *ACS Nano* 2014; **8**: 4580–90.

74. Fernández JA, Morishita T and Toyoda M *et al.* Performance of mesoporous carbons derived from poly(vinyl alcohol) in electrochemical capacitors. *J Power Sources* 2008; **175**: 675–9.
75. Chmiola J, Yushin G and Gogotsi Y *et al.* Anomalous increase in carbon capacitance at pore sizes less than 1 nanometer. *Science* 2006; **313**: 1760–3.
76. Simon P and Gogotsi Y. Materials for electrochemical capacitors. *Nat Mater* 2008; **7**: 845–54.
77. Li W, Liu J and Zhao D. Mesoporous materials for energy conversion and storage devices. *Nat Rev Mater* 2016; **1**: 16023.
78. Xia K, Gao Q and Jiang J *et al.* Hierarchical porous carbons with controlled micropores and mesopores for supercapacitor electrode materials. *Carbon* 2008; **46**: 1718–26.
79. Jia S, Wang Y and Xin G *et al.* An efficient preparation of N-doped mesoporous carbon derived from milk powder for supercapacitors and fuel cells. *Electrochim Acta* 2016; **196**: 527–34.
80. Inagaki M, Konno H and Tanaike O. Carbon materials for electrochemical capacitors. *J Power Sources* 2010; **195**: 7880–903.
81. Yan J, Wei T and Shao B *et al.* Electrochemical properties of graphene nanosheet/carbon black composites as electrodes for supercapacitors. *Carbon* 2010; **48**: 1731–7.
82. Lei Z, Christov N and Zhao XS *et al.* Intercalation of mesoporous carbon spheres between reduced graphene oxide sheets for preparing high-rate supercapacitor electrodes. *Energy Environ Sci* 2011; **4**: 1866–73.
83. Qiu L, Yang X and Gou X *et al.* Dispersing carbon nanotubes with graphene oxide in water and synergistic effects between graphene derivatives. *Chemistry—A Eur J* 2010; **16**: 10653–8.
84. Yang Z, Liu M and Zhang C *et al.* Carbon nanotubes bridged with graphene nanoribbons and their use in high-efficiency dye-sensitized solar cells. *Angew Chem Inter Ed* 2013; **52**: 3996–9.
85. Yu D and Dai L. Self-assembled graphene/carbon nanotube hybrid films for supercapacitors. *J Phys Chem Lett* 2010; **1**: 467–70.
86. Sun H, You X and Deng J *et al.* Novel graphene/carbon nanotube composite fibers for efficient wire-shaped miniature energy devices. *Adv Mater* 2014; **26**: 2868–73.
87. Yu D, Goh K and Wang H *et al.* Scalable synthesis of hierarchically structured carbon nanotube–graphene fibres for capacitive energy storage. *Nat Nanotechnol* 2014; **9**: 555–62.
88. You B, Wang L and Yao L *et al.* Three dimensional N-doped graphene–CNT networks for supercapacitor. *Chem Commun* 2013; **49**: 5016–8.
89. Wu Y, Liu S and Zhao K *et al.* Facile synthesis of 3D graphene hydrogel/carbon nanofibers composites for supercapacitor electrode. *ECS Solid State Letters* 2015; **4**: M23–5.
90. Feng X, Liang Y and Zhi L *et al.* Synthesis of microporous carbon nanofibers and nanotubes from conjugated polymer network and evaluation in electrochemical capacitor. *Adv Funct Mater* 2009; **19**: 2125–9.
91. Sun G, Zhang X and Lin R *et al.* Hybrid fibers made of molybdenum disulfide, reduced graphene oxide, and multi-walled carbon nanotubes for solid-state, flexible, asymmetric supercapacitors. *Angew Chem Int Ed* 2015; **54**: 4651–6.
92. Sun G, Liu J and Zhang X *et al.* Fabrication of ultralong hybrid microfibers from nanosheets of reduced graphene oxide and transition-metal dichalcogenides and their application as supercapacitors. *Angew Chem Int Ed* 2014; **53**: 12576–80.
93. Cao X, Zheng B and Shi W *et al.* Reduced graphene oxide-wrapped MoO_3 composites prepared by using metal-organic frameworks as precursor for all-solid-state flexible supercapacitors. *Adv Mater* 2015; **27**: 4695–701.
94. Zhou W, Cao X and Zeng Z *et al.* One-step synthesis of Ni_3S_2 nanorod@$Ni(OH)_2$ nanosheet core–shell nanostructures on a threedimensional graphene network for high-performance supercapacitors. *Energy Environ Sci* 2013; **6**: 2216–21.
95. Obreja VVN. On the performance of supercapacitors with electrodes based on carbon nanotubes and carbon activated material: a review. *Physica E: Low-dimen Sys Nanostruct* 2008; **40**: 2596–605.
96. Bai X, Hu X and Zhou S *et al.* In situ polymerization and characterization of grafted poly (3,4-ethylenedioxythiophene)/multiwalled carbon nanotubes composite with high electrochemical performances. *Electrochim Acta* 2013; **87**: 394–400.
97. Paul S, Choi KS and Lee DJ *et al.* Factors affecting the performance of supercapacitors assembled with polypyrrole/multi-walled carbon nanotube composite electrodes. *Electrochim Acta* 2012; **78**: 649–55.
98. Li H, Wang J and Chu Q *et al.* Theoretical and experimental specific capacitance of polyaniline in sulfuric acid. *J Power Sources* 2009; **190**: 578–86.
99. Liu J, Sun J and Gao L. A promising way to enhance the electrochemical behavior of flexible single-walled carbon nanotube/polyaniline composite films. *J Phys Chem C* 2010; **114**: 19614–20.
100. Chen X, Lin H and Chen P *et al.* Smart, stretchable supercapacitors. *Adv Mater* 2014; **26**: 4444–9.
101. Jang JH, Kato A and Machida K *et al.* Supercapacitor performance of hydrous ruthenium oxide electrodes prepared by electrophoretic deposition. *J Electrochem Soc* 2006; **153**: A321–8.
102. Chen S, Zhu J and Han Q *et al.* Shape-controlled synthesis of one-dimensional MnO_2 via a facile quick-precipitation procedure and its electrochemical properties. *Cryst Grow Des* 2009; **9**: 4356–61.
103. Yuan C, Zhang X and Su L *et al.* Facile synthesis and self-assembly of hierarchical porous NiO nano/micro spherical superstructures for high performance supercapacitors. *J Mater Chem* 2009; **19**: 5772–7.
104. Nagarajan N, Humadi H and Zhitomirsky I. Cathodic electrodeposition of MnOx films for electrochemical supercapacitors. *Electrochim Acta* 2006; **51**: 3039–45.
105. Patil UM, Gurav and Fulari Vj KV *et al.* Characterization of honeycomb-like 'β-Ni(OH)2' thin films synthesized by chemical bath deposition method and their supercapacitor application. *J Power Sources* 2009; **188**: 338–42.
106. Lang J, Kong L and Wu W *et al.* A facile approach to the preparation of loose-packed $Ni(OH)_2$ nanoflake materials for electrochemical capacitors. *Solid State Electrochem* 2009; **13**: 333–40.
107. Reddy ALM and Ramaprabhu S. Nanocrystalline metal oxides dispersed multiwalled carbon nanotubes as supercapacitor electrodes. *J Phys Chem C* 2007; **111**: 7727–34.
108. Kim I, Kim J and Kim K. Electrochemical characterization of electrochemically prepared ruthenium oxide/carbon nanotube electrode for supercapacitor application. *Electrochem Solid-St Lett* 2005; **8**: A369–72.
109. Huang M, Zhang Y and Li F *et al.* Self-assembly of mesoporous nanotubes assembled from interwoven ultrathin birnessite-type MnO_2 nanosheets for asymmetric supercapacitors. *Sci Rep* 2014; **4**: 3878.
110. Amade R, Jover E and Caglar B *et al.* Optimization of MnO_2/vertically aligned carbon nanotube composite for supercapacitor application. *J Power Sources* 2011; **196**: 5779–83.
111. Li L, Hu ZA and An N *et al.* Facile synthesis of MnO_2/CNTs composite for supercapacitor electrodes with long cycle stability. *J Phys Chem C* 2014; **118**: 22865–72.

112. Ren J, Li L and Chen C *et al.* Twisting carbon nanotube fibers for both wire-shaped micro-supercapacitor and micro-battery. *Adv Mater* 2013; **25**: 1155–9.
113. Wang H, Hao Q and Yang X *et al.* Twisting carbon nanotube fibers for both wire-shaped micro-supercapacitor and micro-battery. *Electrochem Commun* 2009; **11**: 1158–61.
114. Xu J, Wang K and Zu SZ *et al.* Hierarchical nanocomposites of polyaniline nanowire arrays on graphene oxide sheets with synergistic effect for energy storage. *ACS Nano* 2010; **4**: 5019–26.
115. Yan J, Wei T and Shao B *et al.* Preparation of a graphene nanosheet/polyaniline composite with high specific capacitance. *Carbon* 2010; **48**: 487–93.
116. Li L, Raji ARO and Fei H *et al.* Nanocomposite of polyaniline nanorods grown on graphene nanoribbons for highly capacitive pseudocapacitors. *ACS Appl Mater Inter* 2013; **5**: 6622–7.
117. Giri S, Ghosh D and Das CK. In situ synthesis of cobalt doped polyaniline modified graphene composites for high performance supercapacitor electrode material. *J Electroanal Chem* 2013; **697**: 32–45.
118. Tai Z, Yan X and Xue Q. Three-dimensional graphene/polyaniline composite hydrogel as supercapacitor electrode. *J Electrochem Soc* 2012; **159**: A1702–9.
119. Lee T, Yun T and Park B *et al.* Hybrid multilayer thin film supercapacitor of graphene nanosheets with polyaniline: importance of establishing intimate electronic contact through nanoscale blending. *J Mater Chem* 2012; **22**: 21092–9.
120. Lee JW, Lee JU and Jo JW *et al.* In-situ preparation of graphene/poly(styrenesulfonic acid-graft-polyaniline) nanocomposite via direct exfoliation of graphite for supercapacitor application. *Carbon* 2016; **105**: 191–8.
121. Liu J, An J and Ma Y *et al.* Synthesis of a graphene-polypyrrole nanotube composite and its application in supercapacitor electrode. *J Electrochem Soc* 2012; **159**: A828–33.
122. Konwer S, Boruah R and Dolui SK. Studies on conducting polypyrrole/graphene oxide composites as supercapacitor electrode. *J Electron Mater* 2011; **40**: 2248–55.
123. Li J, Xie H and Li Y. Fabrication of graphene oxide/polypyrrole nanowire composite for high performance supercapacitor electrodes. *J Power Sources* 2013; **241**: 388–95.
124. Zhang LL, Zhao S and Tian XN *et al.* Layered graphene oxide nanostructures with sandwiched conducting polymers as supercapacitor electrodes. *Langmuir* 2010; **26**: 17624–8.
125. Zhao Y, Liu J and Hu Y *et al.* Highly compression-tolerant supercapacitor based on polypyrrole-mediated graphene foam electrodes. *Adv Mater* 2013; **25**: 591–5.
126. Mini PA, Balakrishnan A and Nair SV *et al.* Highly super capacitive electrodes made of graphene/poly(pyrrole). *Chem Commun* 2011; **47**: 5753–5.
127. Chen S, Zhu J and Wu X *et al.* Graphene oxide—MnO_2 nanocomposites for supercapacitors. *ACS Nano* 2010; **4**: 2822–30.
128. Zhang B, Yu B and Zhou F *et al.* Polymer brush stabilized amorphous MnO_2 on graphene oxide sheets as novel electrode materials for high performance supercapacitors. *J Mater Chem A* 2013; **1**: 8587–92.
129. Zhao X, Zhang L and Murali S *et al.* Incorporation of manganese dioxide within ultraporous activated graphene for high-performance electrochemical capacitors. *ACS Nano* 2012; **6**: 5404–12.
130. Yan J, Fan Z and Wei T *et al.* Fast and reversible surface redox reaction of graphene-MnO_2 composites as supercapacitor electrode. *Carbon* 2010; **48**: 3825–33.
131. Zhu L, Zhang S and Cui Y *et al.* One step synthesis and capacitive performance of graphene nanosheets/Mn_3O_4 composite. *Electrochim Acta* 2013; **89**: 18–23.
132. Gao H, Xiao F and Ching CB *et al.* Flexible all-solid-state asymmetric supercapacitors based on free-standing carbon nanotube/graphene and Mn_3O_4 nanoparticle/graphene paper electrodes. *ACS Appl Mater Interfaces* 2012; **4**: 7020–6.
133. Lee KH, Lee YW and Lee SW *et al.* Ice-templated self-assembly of $VOPO_4$-graphene nanocomposites for vertically porous 3D supercapacitor electrodes. *Sci Rep* 2015; **5**: 13696.
134. Wu ZS, Wang DW and Ren W *et al.* Anchoring hydrous RuO_2 on graphene sheets for high-performance electrochemical capacitors. *Adv Funct Mater* 2010; **20**: 3595–602.
135. Yan J, Wei T and Qiao W *et al.* Rapid microwave-assisted synthesis of graphene nanosheet/Co_3O_4 composite for supercapacitors. *Electrochim Acta* 2010; **55**: 6973–8.
136. Wang X, Liu S and Wang H *et al.* Facile and green synthesis of Co_3O_4 nanoplates/graphene nanosheets composite for supercapacitor. *J Solid State Electrochem* 2012; **16**: 3593–602.
137. Sun CY, Zhu YG and Zhu TJ *et al.* $Co(OH)_2$/graphene sheet-on-sheet hybrid as high-performance electrochemical pseudocapacitor electrodes. *J Solid State Electrochem* 2013; **17**: 1159–65.
138. Yan J, Fan Z and Sun W *et al.* Advanced asymmetric supercapacitors based on $Ni(OH)_2$ /graphene and porous graphene electrodes with high energy density. *Adv Funct Mater* 2012; **22**: 2632–41.
139. Wang H, Casalongue HS and Liang Y *et al.* $Ni(OH)_2$ nanoplates grown on graphene as advanced electrochemical pseudocapacitor materials. *J Am Chem Soc* 2010; **132**: 7472–7.
140. Lee KK, Deng S and Fan H *et al.* α-Fe_2O_3 nanotubes-reduced graphene oxide composites as synergistic electrochemical capacitor materials. *Nanoscale* 2012; **4**: 2958–61.
141. Sun X, Xie M and Wang G *et al.* Atomic layer deposition of TiO_2 on graphene for supercapacitors. *J Electrochem Soc* 2012; **159**: A364–9.
142. Wang J, Gao Z and Li Z *et al.* Green synthesis of graphene nanosheets/ZnO composites and electrochemical properties. *J Solid State Chem* 2011; **184**: 1421–7.
143. Fang Y, Luo B and Jia Y *et al.* Renewing functionalized graphene as electrodes for high-performance supercapacitors. *Adv Mater* 2012; **24**: 6348–55.
144. Zhang X, Sun S and Sun X *et al.* Plasma-induced, nitrogen-doped graphene-based aerogels for high-performance supercapacitors. *Light: Sci Appl* 2016; **5**: e16130.
145. Xu Y, Lin Z and Huang X *et al.* Functionalized graphene hydrogel-based high-performance supercapacitors. *Adv Mater* 2013; **25**: 5779–84.
146. Zhang N, Fu C and Liu D *et al.* Three-dimensional pompon-like MnO_2/graphene hydrogel composite for supercapacitor. *Electrochimica Acta* 2016; **210**: 804–11.
147. Wu S, Chen W and Yan L. Fabrication of a 3D MnO_2/graphene hydrogel for high-performance asymmetric supercapacitors. *J Mater Chem A* 2014; **2**: 2765–72.
148. Wu Q, Sun Y and Bai H *et al.* High-performance supercapacitor electrodes based on graphene hydrogels modified with 2-aminoanthraquinone moieties. *Phys Chem Chem Phys* 2011; **13**: 11193–8.
149. Yang Y, Liang Y and Zhang Y *et al.* Three-dimensional graphene hydrogel supported ultrafine RuO_2 nanoparticles for supercapacitor electrodes. *New J Chem* 2015; **39**: 4035–40.

150. Moussa M, Zhao Z and El-Kady MF *et al.* Free-standing composite hydrogel films for superior volumetric capacitance. *J Mater Chem A* 2015; **3**: 15668–74.
151. Wang H, Xu Z and Yi H *et al.* One-step preparation of single-crystalline Fe_2O_3 particles/graphenecomposite hydrogels as high performance anode materials for supercapacitors. *Nano Energy* 2014; **7**: 86–96.
152. Sun Y, Wu Q and Shi G *et al.* Supercapacitors based on self-assembled graphene organogel. *Phys Chem Chem Phys* 2011; **13**: 17249–54.
153. Xiong Z, Liao C and Wand X. A self-assembled macroporous coagulation graphene network with high specific capacitance for supercapacitor applications. *J Mater Chem A* 2014; **2**: 19141–4.
154. Hao L, Luo B and Li X *et al.* Terephthalonitrile-derived nitrogen-rich networks for high performance supercapacitors. *Energy Environ Sci* 2012; **5**: 9747–51.
155. Liang Y, Feng X and Zhi L *et al.* A simple approach towards one-dimensional mesoporous carbon with superior electrochemical capacitive activity. *Chem Commun* 2009; 809–11.
156. Xu Y, Tao Y and Zheng X *et al.* A metal-free supercapacitor electrode material with a record high volumetric capacitance over 800 F cm-3. *Adv Mater* 2015; **27**: 8082–7.
157. Ren TZ, Liu L and Zhang Y *et al.* Nitric acid oxidation of ordered mesoporous carbons for use in electrochemical supercapacitors. *J Solid State Electrochem* 2013; **17**: 2223–33.
158. Wang L., Yu J and Dong X *et al.* Three-dimensional macroporous carbon/Fe_3O_4-doped porous carbon nanorods for high-performance supercapacitor. *ACS Sustainable Chem Eng* 2016; **4**: 1531–7.
159. Yan Y, Cheng Q and Zhu Z *et al.* Controlled synthesis of hierarchical polyaniline nanowires/ordered bimodal mesoporous carbon nanocomposites with high surface area for supercapacitor electrodes. *J Power Sources* 2013; **240**: 544–50.
160. Deng Y, Xie Y and Zoua K *et al.* Review on recent advances in nitrogen-doped carbons: preparations and applications in supercapacitors. *J Mater Chem A* 2016; **4**: 1144–77.
161. Dai L, Xue Y and Qu L *et al.* Metal-free catalysts for oxygen reduction reaction. *Chem Rev* 2015; **115**: 4823–92.
162. Rennie AJR and Hall PJ. Nitrogen-enriched carbon electrodes in electrochemical capacitors: investigating accessible porosity using CM-SANS. *Phys Chem Chem Phys* 2013; **15**: 16774–8.
163. Yan J, Wei T and Fan Z *et al.* Preparation of graphene nanosheet/carbon nanotube/polyaniline composite as electrode material for supercapacitors. *J Power Sources* 2010; **195**: 3041–5.
164. Kim KS and Park SJ. Synthesis and high electrochemical capacitance of N-doped microporous carbon/carbon nanotubes for supercapacitor. *J Electroanal Chem* 2012; **673**: 58–64.
165. Cheng Q, Tang J and Shinya N *et al.* Polyaniline modified graphene and carbon nanotube composite electrode for asymmetric supercapacitors of high energy density. *J Power Sources* 2013; **241**: 423–8.
166. Jin Y, Chen H and Chen M *et al.* Graphene-patched CNT/MnO_2 nanocomposite papers for the electrode of high-performance flexible asymmetric supercapacitors. *ACS Appl Mater Interfaces* 2013; **5**: 3408–16.
167. Wang G, Tang Q and Bao H *et al.* Synthesis of hierarchical sulfonated graphene/MnO_2/polyaniline ternary composite and its improved electrochemical perrformance. *J Power Sources* 2013; **241**: 231–8.
168. Wu D, Xiao T and Tan X *et al.* High-performance asymmetric supercapacitors based on cobalt chloride carbonate hydroxide nanowire arrays and activated carbon. *Electrochim Acta* 2016; **198**: 1–9.
169. Ratha S, Marri AR and Behera JN *et al.* High-energy-density supercapacitors based on patronite/single-walled carbon nanotubes/reduced graphene oxide hybrids. *Eur J Inorg Chem* 2016; **2016**: 259–65.
170. Zhang Y, Si L and Zhou B *et al.* Synthesis of novel graphene oxide/pristine graphene/polyaniline ternary composites and application to supercapacitor. *Chem Eng J* 2016; **288**: 689–700.
171. Du F, Yu D and Dai L *et al.* Preparation of tunable 3D pillared carbon nanotube-graphene networks for high-performance capacitance. *Chem Mater* 2011; **23**: 4810–6.
172. Fan Z, Yan J and Zhi L *et al.* A three-dimensional carbon nanotube/graphene sandwich and Its application as electrode in supercapacitors. *Adv Mater* 2010; **22**: 3723–8.
173. Simon P and Gogotsi Y. Materials for electrochemical capacitors. *Nat Mater* 2008; **7**: 845–54.
174. Zhao X, Johnston C and Grant PS. A novel hybrid supercapacitor with a carbon nanotube cathode and an iron oxide/carbon nanotube composite anode. *J Mater Chem* 2009; **19**: 8755–60.
175. Dubal DP, Ayyad O and Ruiz V *et al.* Hybrid energy storage: the merging of battery and supercapacitor chemistries. *Chem Soc Rev* 2015; **44**: 1777–90.
176. Kadya MFE, Ihnsa M and Lia M *et al.* Engineering three-dimensional hybrid supercapacitors and microsupercapacitors for high-performance integrated energy storage. *Proc Natl Acad Sci U S A* 2015; **112**: 4233–8.
177. Ma Y, Chang H and Zhang M *et al.* Graphene-based materials for lithium-ion hybrid supercapacitors. *Adv Mater* 2015; **27**: 5296–308.
178. El-Kadya MF, Ihns M and Li M *et al.* Engineering three-dimensional hybrid supercapacitors and microsupercapacitors for high-performance integrated energy storage. *Proc Natl Acad Sci U S A* 2015; **112**: 4233–8.
179. Zhang F, Zhang T and Yang X *et al.* A high-performance supercapacitor-battery hybrid energy storage device based on graphene-enhanced electrode materials with ultrahigh energy density. *Energy Environ Sci* 2013; **6**: 1623–32.
180. Lim E, Kim H and Jo C *et al.* Advanced hybrid supercapacitor based on a mesoporous niobium pentoxide/carbon as high-performance anode. *ACS Nano* 2014; **8**: 8968–78.
181. Li B, Dai F and Xiao Q *et al.* Nitrogen-doped activated carbon for a high energy hybrid supercapacitor. *Energy Environ Sci* 2016; **9**: 102–6.
182. Chen PC, Shen G and Sukcharoenchoke S *et al.* Flexible and transparent supercapacitor based on In_2O_3 nanowire/carbon nanotube heterogeneous films. *Appl Phys Lett* 2009; **94**: 043113 1–3.
183. Nataraj SK, Song Q and Al-Muhtaseb SA *et al.* Thin, flexible supercapacitors made from carbon nanofiber electrodes decorated at room temperature with manganese oxide nanosheets. *J Nanomater* 2013; **272093**: 1–6.
184. Chien CJ, Deora SS and Chang P *et al.* Flexible symmetric supercapacitors based on TiO_2 and carbon nanotubes. *IEEE Transact Nanotechnol* 2011; **10**: 706–9.
185. Zopf SF and Panzer MJ. Integration of UV-cured Ionogel electrolyte with carbon paper electrodes. *AIMS Mater Sci* 2014; **1**: 59–69.
186. Liu Y, Zhou J and Chen L *et al.* Flexible hybrid membranes with $Ni(OH)_2$ nanoplatelets vertically grown on electrospun carbon nanofibers for high-performance supercapacitors. *ACS Appl Mater Interfaces* 2015; **7**: 23515–20.
187. Du L, Yang P and Yu X *et al.* Flexible supercapacitors based on carbon nanotube/MnO_2 nanotube hybrid porous films for wearable electronic devices. *J Mater Chem A* 2014; **2**: 17561–7.
188. Chen T and Dai L. Flexible supercapacitors based on carbon nanomaterials. *J Mater Chem A* 2014; **2**: 10756–75.

189. Yesi Y, Shown I and Ganguly A *et al.* Directly-grown hierarchical carbon nanotube@polypyrrole core-shell hybrid for high-performance flexible supercapacitors. *Chem Sus Chem* 2016; **9**: 370–8.
190. Mitchell E, Jimenez A and Gupta RK *et al.* Ultrathin porous hierarchically textured $NiCo_2O_4$-graphene oxide flexible nanosheets for high-performance supercapacitors. *New J Chem* 2015; **39**: 2181–7.
191. Li M, Tang Z and Leng M *et al.* Flexible solid-state supercapacitor based on graphene-based hybrid films. *Adv Funct Mater* 2014; **24**: 7495–502.
192. Wang Y, Tang S and Vongehr S *et al.* High-performance flexible solid-state carbon cloth supercapacitors based on highly processible N-graphene doped polyacrylic acid/polyaniline composites. *Sci Rep* 2016; **6**: 12883.
193. Aphale A, Maisuria K and Mahapatra MK *et al.* Hybrid electrodes by in-situ integration of graphene and carbon-nanotubes in polypyrrole for supercapacitors. *Sci Rep* 2016; **5**: 14445.
194. Yu N, Yin H and Zhang W *et al.* High-performance fiber-shaped all-solid-state asymmetric supercapacitors based on ultrathin MnO_2 nanosheet/carbon fiber cathodes for wearable electronics. *Adv Energy Mater* 2016; **6**: 1501458.
195. Huang M, Zhang Y and Li F *et al.* Self-assembly of mesoporous nanotubes assembled from interwoven ultrathin birnessite-type MnO_2 nanosheets for asymmetric supercapacitors. *Sci Rep* 2014; **4**: 3878.
196. Xu H, Hu X and Yang H *et al.* Flexible asymmetric micro-supercapacitors based on Bi_2O_3 and MnO_2 nanoflowers: large areal mass promises higher energy density. *Adv Energy Mater* 2015; **5**: 1401882.
197. Xu Y, Li W and Zhang F *et al.* In situ incorporation of FeS nanoparticles/carbon nanosheets composite with an interconnected porous structure as a high-performance anode for lithium ion batteries. *J Mater Chem A* 2016; **4**: 3697–703.
198. He Y, Chen W and Li X *et al.* Freestanding three-dimensional graphene/MnO_2 composite networks as ultralight and flexible supercapacitor electrodes. *ACS Nano* 2013; **7**: 174–82.
199. Zhao Y, Ran W and He J *et al.* High-performance asymmetric supercapacitors based on multilayer MnO_2/graphene oxide nanoflakes and hierarchical porous carbon with enhanced cycling stability. *Small* 2015; **11**: 1310–9.
200. Wu S, Chen W and Yan L. Fabrication of a 3D MnO_2/graphene hydrogel for high-performance asymmetric supercapacitors. *J Mater Chem A* 2014; **2**: 2765–72.
201. Peng L, Peng X and Liu B *et al.* Ultrathin two-dimensional MnO_2/graphene hybrid nanostructures for high-performance, flexible planar supercapacitors. *Nano Lett* 2013; **13**: 2151–7.
202. Yu D, Goh K and Wang H *et al.* Scalable synthesis of hierarchically structured carbon nanotube–graphene fibres for capacitive energy storage. *Nat Nanotechnol* 2014; **9**: 555–62.
203. Veerasubramani GK, Krishnamoorthy K and Pazhamalai P *et al.* Enhanced electrochemical performances of graphene based solid-state flexible cable type supercapacitor using redox mediated polymer gel electrolyte. *Carbon* 2016; **105**: 638–48.
204. Lamberti A, Gigot A and Bianco S *et al.* Self-assembly of graphene aerogel on copper wire for wearable fiber-shaped supercapacitors. *Carbon* 2016; **105**: 649–54.
205. Zhai T, Lu X and Wang F *et al.* MnO_2 nanomaterials for flexible supercapacitors: performance enhancement via intrinsic and extrinsic modification. *Nanoscale Horiz* 2016; **1**: 109–24.
206. Yu C, Masarapu C and Rong J *et al.* Stretchable supercapacitors based on buckled single-walled carbon nanotube macrofilms. *Adv Mater* 2009; **21**: 4793–7.
207. Niu Z, Dong H and Zhu B *et al.* Highly stretchable, integrated supercapacitors based on single-walled carbon nanotube films with continuous reticulate architecture. *Adv Mater* 2013; **25**: 1058–64.
208. Zang J, Cao C and Feng Y *et al.* Stretchable and high-performance supercapacitors with crumpled graphene papers. *Sci Rep* 2014; **4**: 6492.
209. Chen T, Xue Y and Roy AK *et al.* Transparent and stretchable high-performance supercapacitors based on wrinkled graphene electrodes. *ACS Nano* 2014; **8**: 1039–46.
210. Kim W and Kim W. 3 V omni-directionally stretchable one-body supercapacitors based on a single ion–gel matrix and carbon nanotubes. *Nanotechnology* 2016; **27**: 225402.
211. Yun TG, Hwang Bi and Kim D *et al.* Polypyrrole-MnO_2-coated textile-based flexible-stretchable supercapacitor with high electrochemical and mechanical reliability. *ACS Appl Mater Interfaces* 2015; **7**: 9228–34.
212. Pu J, Wang X and Kuang X *et al.* Stretchable microsupercapacitor arrays with a composite honeycomb structure. *IEEE MEMS* 2016; 978–1–5090–1973–1: 1232–5.
213. Yun J, Lim Y and Jang GN *et al.* Stretchable patterned graphene gas sensor driven by integrated micro-supercapacitor array. *Nano Energy* 2016; **19**: 401–14.
214. Yu J, Lu W and Pei S *et al.* Omnidirectionally stretchable high-performance supercapacitor based on isotropic buckled carbon nanotube films. *ACS Nano* 2016; **10**: 5204–11.
215. Choi C, Sim HJ and Spinks GM *et al.* Supercapacitors: elastomeric and dynamic MnO_2/CNT core-shell structure coiled yarn supercapacitor. *Adv Energy Mater* 2016; **6**: 1502119.
216. Yang Z, Deng J and Chen X *et al.* A highly stretchable, fiber-shaped supercapacitor. *Angew Chem Int Ed* 2013; **52**: 13453–7.
217. Chen T, Hao R and Peng H *et al.* High-performance, stretchable, wire-shaped supercapacitors. *Angew Chem Int Ed* 2015; **54**: 618–22.
218. Kanninen P, Luong ND and Sinh LH *et al.* Transparent and flexible high-performance supercapacitors based on single-walled carbon nanotube films. *Nanotechnology* 2016; **27**: 235403.
219. Chen T, Peng H and Durstock M *et al.* High-performance transparent and stretchable all-solid supercapacitors based on highly aligned carbon nanotube sheets. *Sci Rep* 2014; **4**: 3612.
220. Dale A, Brownson C and Banks CE. Fabricating graphene supercapacitors: highlighting the impact of surfactants and moieties. *Chem Commun* 2012; **48**: 1425–7.
221. Zhang LL and Zhao XS. Carbon-based materials as supercapacitor electrodes. *Chem Soc Rev* 2009; **38**: 2520–31.
222. Pandolfo AG and Hollenkamp AF. Carbon properties and their role in supercapacitors. *J Power Sources* 2006; **157**: 11–27.
223. Miller JR, Outlaw RA and Holloway BC. Graphene double-layer capacitor with ac line-filtering performance. *Science* 2010; **329**: 1637–9.
224. Niu C, Sichel EK and Hoch R *et al.* High power electrochemical capacitors based on carbon nanotube electrodes. *Appl Phys Lett* 1997; **70**: 1480–2.
225. Joseph J, Paravannoor A and Nair SV. Supercapacitors based on camphor-derived meso/macroporous carbon sponge electrodes with ultrafast frequency response for ac line-filtering. *J Mater Chem A* 2015; **3**: 14105–8.
226. Miller JR, Outlaw RA and Holloway BC. Graphene double-layer capacitor with ac line-filtering performance. *Science* 2010; **329**: 1637–9.
227. Sheng K, Sun Y and Li C *et al.* Ultrahigh-rate supercapacitors based on eletrochemically reduced graphene oxide for ac line-filtering. *Sci Rep* 2012; **2**: 247.

228. Pech D, Brunet M and Durou H *et al.* Ultrahigh-power micrometre-sized supercapacitors based on onion-like carbon. *Nat Nanotech* 2010; **5**: 651–4.
229. Futaba DN, Hata K and Yanada T *et al.* Shape-engineerable and highly densely packed single-walled carbon nanotubes and their application as super-capacitor electrodes. *Nat Mater* 2006; **5**: 987–94.
230. Rangom Y, Tang X and Nazar LF. Carbon nanotube-based supercapacitors with excellent ac line filtering and rate capability via improved interfacial impedance. *ACS Nano* 2015; **9**: 7248–55.
231. Korenblit Y, Rose M and Kockrick E *et al.* High-rate electrochemical capacitors based on ordered mesoporous silicon carbide-derived carbon. *ACS Nano* 2010; **4**: 1337–44.
232. Lang X, Hirata A and Fujita T *et al.* Nanoporous metal/oxide hybrid electrodes for electrochemical supercapacitors. *Nat Nanotech* 2011; **6**: 232–6.
233. Hou Y, Cheng Y and Hobson T *et al.* Design and synthesis of hierarchical MnO_2 nanospheres/carbon nanotubes/conducting polymer ternary composite for high performance electrochemical electrodes. *Nano Lett* 2010; **10**: 2727–33.
234. Wu ZS, Feng X and Cheng HM. Recent advances in graphene-based planar micro-supercapacitors for on-chip energy storage. *Natl Sci Rev* 2014; **1**: 277–92.
235. Lim J, Maiti UN and Kim NY *et al.* Dopant-specific unzipping of carbon nanotubesfor intact crystalline graphene nanostructures. *Nat Commun* 2016; **7**: 10364.
236. Wei H, Wei S and Tian W *et al.* Fabrication of thickness controllable free-standing sandwich-structured hybrid carbon film for high-rate and high-power supercapacitor. *Sci Rep* 2014; **4**: 7050.
237. Lin J, Zhang CG and Yan Z *et al.* 3-dimensional graphene carbon nanotube carpet-based microsupercapacitors with high electrochemical performance. *Nano Lett* 2013; **13**: 72–8.